Bulletin of Volcanology

Volcanic activity and gas emissions along the South Sandwich arc

--Manuscript Draft--

Manuscript Number:	
Full Title:	Volcanic activity and gas emissions along the South Sandwich arc
Article Type:	Research Article
Corresponding Author:	Emma J Liu, PhD University College London UNITED KINGDOM
Corresponding Author Secondary Information:	
Order of Authors:	Emma J Liu, PhD
	Kieran Wood
	Alessandro Aiuppa
	Marcello Bitetto
	Gaetano Giudice
	Tobias Fischer
	Brendan McCormick Kilbride
	Terry Plank
	Tom Hart
Funding Information:	Leverhulme Trust (Early Career Fellowship) — Dr Emma J Liu
	MUIR (2017LMNLAW) — Prof Alessandro Aiuppa
	Quark Expeditions Ltd (Public Donations) — Dr Tom Hart
	Government of South Georgia and the South Sandwich Islands — Dr Tom Hart
Abstract:	The South Sandwich Volcanic Arc is one of the most remote and enigmatic arcs on Earth. Sporadic observations from rare cloud-free satellite images—and even rarer in situ reports—provide tantalising glimpses of a dynamic arc system characterised by persistent gas emissions and frequent eruptive activity. However, our understanding of the state of active volcanic activity along this arc is hugely incomplete compared to arcs globally. Here, we present detailed geological and volcanological observations made during an expedition to the South Sandwich Islands in January 2020. We report in situ measurements of gas chemistry, emission rate, and carbon isotope composition from along the arc. We show that Mt Michael on Saunders Island is a persistent source of gas emissions, releasing 145 ± 59 t d -1 SO 2 and 267 ± 112 t d -1 CO 2 in a plume characterised by a CO 2 /SO 2 ratio of 1.8 ± 0.2. Fumarolic outgassing is prevalent in the active centres of Candlemas and Bellingshausen islands. Carbon isotope measurements of dilute plume and fumarole gases from along the arc suggest a magmatic δ 13 C of -4.5 ± 2.0 ‰, which we discuss in the context of mixing between mantle carbon and a recycled subduction component composed of carbon-poor sediment and altered crust.
Suggested Reviewers:	Philip Leat British Antarctic Survey ptle@bas.ac.uk Dr Leat has authored much of the fundamental geological and petrological literature on the South Sandwich Islands.
	John Smellie University of Leicester

	jls55@le.ac.uk Prof Smellie is one of very few volcanologists/geologists who have visited the South Sandwich Islands in person, and published some of the fundamental work in this region.
	Matt Patrick USGS mpatrick@usgs.gov Dr Patrick has published satellite remote sensing observations of the South Sandwich arc and so has a comprehensive overall understanding of volcanic activity in the region, from a slightly different perspective than the other two suggested reviewers.
Author Comments:	

LONDON'S GLOBAL UNIVERSITY

Editor, *Bulletin of Volcanology*
Submission date: 13 July 2020

Dear Editor,

We are pleased to submit the manuscript "Volcanic activity and gas emissions along the South Sandwich arc" for consideration as a Research Article by Bulletin of Volcanology.

In this study, we present detailed geological and volcanological observations from the remote South Sandwich volcanic arc. Building on previous petrological and remote sensing studies in the region, we focus on volcanic gas emissions and report the first in situ measurements of gas chemistry, emission rate, and carbon isotope composition from along this remote arc. We show that Mt Michael on Saunders Island is a persistent source of gas emissions, releasing 145 ± 59 t d^{-1} SO_2 and 267 ± 112 t d^{-1} CO_2 in a plume characterised by a CO_2/SO_2 ratio of 1.8 ± 0.2, which we discuss in the context of recently published global syntheses. Fumarolic outgassing is prevalent in the active centres of Candlemas and Bellingshausen islands. Carbon isotope measurements of dilute plume and fumarole gases from along the arc suggest a magmatic $\delta^{13}C$ of -4.5 ± 2.0 ‰, which we discuss in the context of mixing between mantle carbon and a recycled subduction component composed of carbon-poor sediment and altered crust. The South Sandwich volcanic arc represents an ideal tectonic setting in which to explore the geochemical processes of an exceptionally young arc, and this study will provide a comprehensive foundation for future volcanological work in the region.

Each of the authors confirm that this manuscript has not been previously published and is not currently under consideration by any other journal. All authors have approved the contents of this paper, and confirm there are no ethical issues or conflicts of interest to disclose.

Sincerely,

Dr Emma Liu

University College London
5 Gower Place, London, WC1E 6BS
emma.liu@ucl.ac.uk

Volcanic activity and gas emissions along the South Sandwich arc

Emma J. Liu[1*], Kieran Wood[2], Alessandro Aiuppa[3], Gaetano Giudice[4], Marcello Bitetto[3], Tobias Fischer[5], Brendan McCormick Kilbride[6], Terry Plank[7], Tom Hart[8]

[1]Department of Earth Sciences, University College London, 5 Gower Place, London, UK, WC1E 6BS
*(emma.liu@ucl.ac.uk).
[2]Aerospace Engineering, University of Bristol, Bristol, UK, BS8 1TR.
[3]Dipartimento di Scienze della Terra e del Mare, University of Palermo, Palermo, Italy
[4]INGV, Sezione di Catania, Italy
[5]Department of Earth and Planetary Sciences, University of New Mexico, Albuquerque, US
[6]Department of Earth and Environmental Sciences, University of Manchester, Williamson Building, Oxford Road, Manchester, UK, M13 9QQ
[7]Lamont-Doherty Earth Observatory, Columbia University, New York, US
[8]Department of Zoology, University of Oxford, South Parks Road, Oxford, UK, OX1 3SZ.

ABSTRACT

The South Sandwich Volcanic Arc is one of the most remote and enigmatic arcs on Earth. Sporadic observations from rare cloud-free satellite images—and even rarer in situ reports—provide tantalising glimpses of a dynamic arc system characterised by persistent gas emissions and frequent eruptive activity. However, our understanding of the state of active volcanic activity along this arc is hugely incomplete compared to arcs globally. Here, we present detailed geological and volcanological observations made during an expedition to the South Sandwich Islands in January 2020. We report in situ measurements of gas chemistry, emission rate, and carbon isotope composition from along the arc. We show that Mt Michael on Saunders Island is a persistent source of gas emissions, releasing 145 ± 59 t d^{-1} SO_2 and 267 ± 112 t d^{-1} CO_2 in a plume characterised by a CO_2/SO_2 ratio of 1.8 ± 0.2. Fumarolic outgassing is prevalent in the active centres of Candlemas and Bellingshausen islands. Carbon isotope measurements of dilute plume and fumarole gases from along the arc suggest a magmatic $\delta^{13}C$ of -4.5 ± 2.0 ‰, which we discuss in the context of mixing between mantle carbon and a recycled subduction component composed of carbon-poor sediment and altered crust.

INTRODUCTION

The volcanoes of the South Sandwich volcanic arc (SSVA) are a significant source of tephra to the South Atlantic (Ninkovich et al., 1964) and the Antarctic mainland (Smellie, 1999; Basile et al., 2001) and yet their eruptive processes remain enigmatic compared to other arcs globally. The relatively recent development of the SSVA over the past 10 million years has been closely linked with the formation of the Drake Passage (Barker, 1995; Vanneste and Larter, 2002; Leat et al., 2013, 2016), making this one of the youngest known volcanic arcs on Earth, and therefore one of the most critical for understanding

the early stages of arc geochemical evolution. Records of historical activity are hugely incomplete, with in situ observations contributed by only a handful of expeditions (e.g., Holdgate and Baker, 1979; Smellie et al., 1998; Derrien et al, 2019). Much of the monitoring data collected over the past two decades derive from satellite remote sensing observations (Lachlan-Cope et al., 2001; Patrick et al., 2005; Patrick and Smellie, 2013; Gray et al., 2019), and yet even these are restricted to rare, cloud-free images. Satellite observations reveal persistent passive outgassing at many of the SSVA volcanoes, punctuated by sporadic explosive emissions, suggesting that the arc could be a significant source of volatiles to our atmosphere. Petrological constraints on magmatic volatile content are lacking, as are data on the composition and flux of emitted gases. Here, we present geological and volcanological observations made during an expedition to the South Sandwich Islands in January 2020. We report measurements of gas chemistry, emission rate, and carbon isotope signature from along the SSVA. Together, these observations contribute a comprehensive view of the 'state of the arc', providing foundation for future targeted studies.

BACKGROUND

Tectonic and ecological significance

The South Sandwich volcanic arc (SSVA) is situated on the leading edge of the South Sandwich microplate, bounded to the west by the East Scotia Ridge (ESR) back-arc spreading centre and to the east by the South Sandwich Trench (Fig. 1; Barker, 1970; Larter et al., 2003). Seafloor magnetic anomalies record continuous W-E spreading at the ESR since at least ~15 Ma, initially at a full spreading rate of ~27 mm yr^{-1} until ~1.7 Ma when spreading accelerated to the current rate of 63–71 mm yr^{-1} (Barker, 1995; Livermore et al., 1997; Larter et al., 2003; Thomas et al., 2003). The SSVA is built largely on oceanic crust that formed at the ESR ~10 Ma (Barker, 1995; Larter et al., 2003) and is consequently one of the youngest volcanic arcs active today. The crust beneath the SSVA is relatively thin at 16–20 km compared to arcs globally (~30 km on average), consistent with its young age and extensional regime due to back-arc spreading (e.g., Larter et al., 2003; Calvert, 2011).

The southern end of the SSVA is bounded by the South Sandwich fracture zone, an active transform fault accommodating dextral motion between the Antarctic and South Sandwich plates (Barker, 1995; Thomas et al., 2003; Giner-Robles et al., 2009). At the northern end of the arc, focal mechanisms associated with enhanced seismicity suggest that the underthrust plate is being torn at depth to accommodate subduction (Brett, 1977; Giner-Robles et al., 2009). Upper mantle seismic anisotropy from shear-wave splitting reveals a strain field that describes westward mantle flow into the back-arc region from the north and south (Livermore et al., 1997; Müller, 2001; Müller et al., 2008), consistent with the enriched Atlantic mantle signatures observed in erupted basalts from the northern- and southern-most segments of the ESR (Leat et al., 2004).

Magmatism along the SSVA is the expression of westward oceanic-oceanic subduction of the South American Plate beneath the South Sandwich microplate. Plate convergence is accommodated by subduction rates of 69 ± 11 mm yr^{-1} (north) to 71 ± 10.8 mm yr^{-1} (south), associated with eastward roll-back of the trench (Thomas et al., 2003; Smalley et al., 2007). The age of subducted crust entering the trench from the South American plate varies from ~83 Ma in the north to ~27 Ma in the south (Barker, 1995). Almost all of the sediment entering the trench is subducted, and a well-developed accretionary prism has not been established (Vanneste and Larter, 2002). A sedimentary section from site 701 (Ocean Drilling Programme, ODP 701; Fig. 1) shows that the pelagic sediment north of the arc is carbon-poor overall (Ciesielski et al., 1988). From top to bottom, the pelagic sequence from ODP 701 exposes three main units: ~245 m of diatomaceous ooze, with intervals of siliceous clay-rich muds and volcanic ash; ~200 m of diatom-rich clay/mud, with lesser volcanic ash; and ~30 m of indurated nannofossil chalk—of mid to late Eocene age—overlying amygdaloidal olivine basalt basement (Ciesielski et al, 1988; Vervoort et al., 2011). Sediment thicknesses are thinner immediately east of the arc (~200 m on average; Plank and Langmuir, 1998). Dredge samples of oceanic crust from the South Sandwich Trench (Pearce et al., 2000) and the American-Antarctic Ridge to the east (Lawver and Dick, 1983) are dominated by exposed ultramafic material—serpentinised peridotites, harzburgites, dunites and gabbros—typical of slow-spreading tectonic settings.

Erupted magma compositions range from basaltic to silicic and populate both tholeiitic and calk-alkaline trends; tholeiitic basalts are by far the most abundant (Baker, 1978; Pearce et al., 1995). Overall, the SSVA is considered a type example of early subduction zone magmatism (Baker, 1978). Trace element systematics suggest a variable, element-specific subduction component from altered oceanic crust (Pearce et al., 1995). Boron isotope compositions ($\delta^{11}B$) for SSI lavas are among the highest reported for mantle-derived lavas, suggesting substantial subduction erosion of serpentinised forearc material (Tonarini et al., 2011). Rates of terrigenous erosion from the SSI volcanoes and forearc are high, supplying large amounts of volcaniclastic material eastwards towards the trench (Leat et al., 2010; Tonarini et al., 2011). Overall, the carbon-poor nature of the sediments entering the trench lead to low predicted CO_2/SO_2 ratios ~1.2 in the corresponding arc emissions based on trace element proxies (Aiuppa et al., 2019).

The South Sandwich Islands (SSI) represent the emergent portions of deep-rooted volcanic edifices that comprise the arc front and extend to depths of 2000–3000 m below the sea floor (Leat et al., 2016, 2013, 2010). From north to south along the arc, the volcanic centres include Protector Seamounts (submerged), Zavodovski, Visokoi, Candlemas group (Candlemas and Vindication), Saunders, Montagu, Bristol, Southern Thule group (Bellingshausen, Cook, and Thule), and Kemp and Adventure calderas (submerged). Since 1900, expressions of active volcanism (ranging from sporadic fumaroles to explosive eruptions) have been reported from all but Vindication, which represents the eroded remnants of an ancient stratovolcano. Volcanic edifices are constructed from layers of pyroclastic material and lavas (Baker, 1978; Holdgate and Baker, 1979; Leat et al., 2003; Smellie et al.,

1998). Bathymetric surveys reveal numerous mass flow deposits associated with the submarine flanks of the SSI volcanoes (Leat et al., 2013, 2010). Active seafloor hydrothermal venting, important for sustaining chemosynthetic communities, has been reported from Kemp and Adventure calderas in the southern section of the arc and from the Protector Seamount region in the north (Boschen et al., 2013; Linse et al., 2019). The SSI are located south of the Antarctic Circumpolar Current and the topographic profile of the arc strongly influences the path of oceanographic currents (Garabato et al., 2002).

The South Sandwich Islands have a polar climate, with heavy snowfall in winter and frequent strong winds and storm swells year-round. Terrestrial flora is scarce, dominated by mosses and lichens (Convey et al., 2000; Hart and Convey, 2018). However, the islands are breeding grounds for globally-significant populations of seabirds, notably penguins (Hart and Convey, 2018). At the most recent census in 2011, the SSI contain almost half of the world's population of Chinstrap penguins (Lynch et al., 2016); 600,000 pairs are reported from Zavodovski Island alone, together with a further ~95,000 pairs of Macaroni penguins, and >125,000 pairs of Adelie penguins. The islands are administered as a UK Overseas Territory by the Government of South Georgia and the South Sandwich Islands. In response to calls for long term management of the fishery and dependent wildlife, South Georgia and SSI were declared a Marine Protected Area in 2012, which was further expanded in 2019 (Marine Protected Areas Order, 2013, 2019). Recent volcanic eruptions in the SSI are likely to have had significant and ongoing impacts on local terrestrial and marine ecosystems, through immediate disturbance, deposition of pyroclastic material (mostly as volcanic ash) and from persistent passive degassing. Historic volcanic eruptions elsewhere in the Antarctic have caused mass mortality in penguin colonies (Roberts et al., 2017).

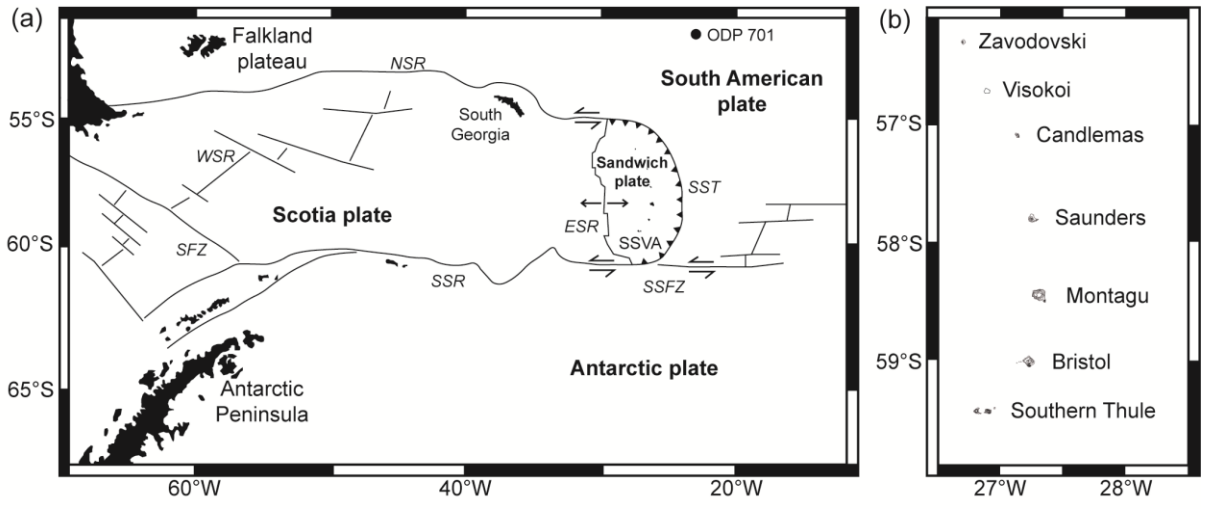

Figure 1: Tectonic setting of the South Sandwich Islands volcanic arc (redrawn from Leat et al., 2016). East Scotia Ridge (ESR), West Scotia Ridge (WSR), South Scotia Ridge (SSR), North Scotia Ridge (NSR), Shackleton Fracture Zone (SFZ), South Sandwich Trench (SST), South Sandwich Fracture Zone

(SSFZ), and South Sandwich Volcanic Arc (SSVA). Location of the ODP Site 701 (Leg 114) sediment core (Ciesielski et al, 1988). (b) Magnified view of the SSVA showing subaerial islands. Topographic data extracted from WorldDEM™ (Airbus Space and Defence).

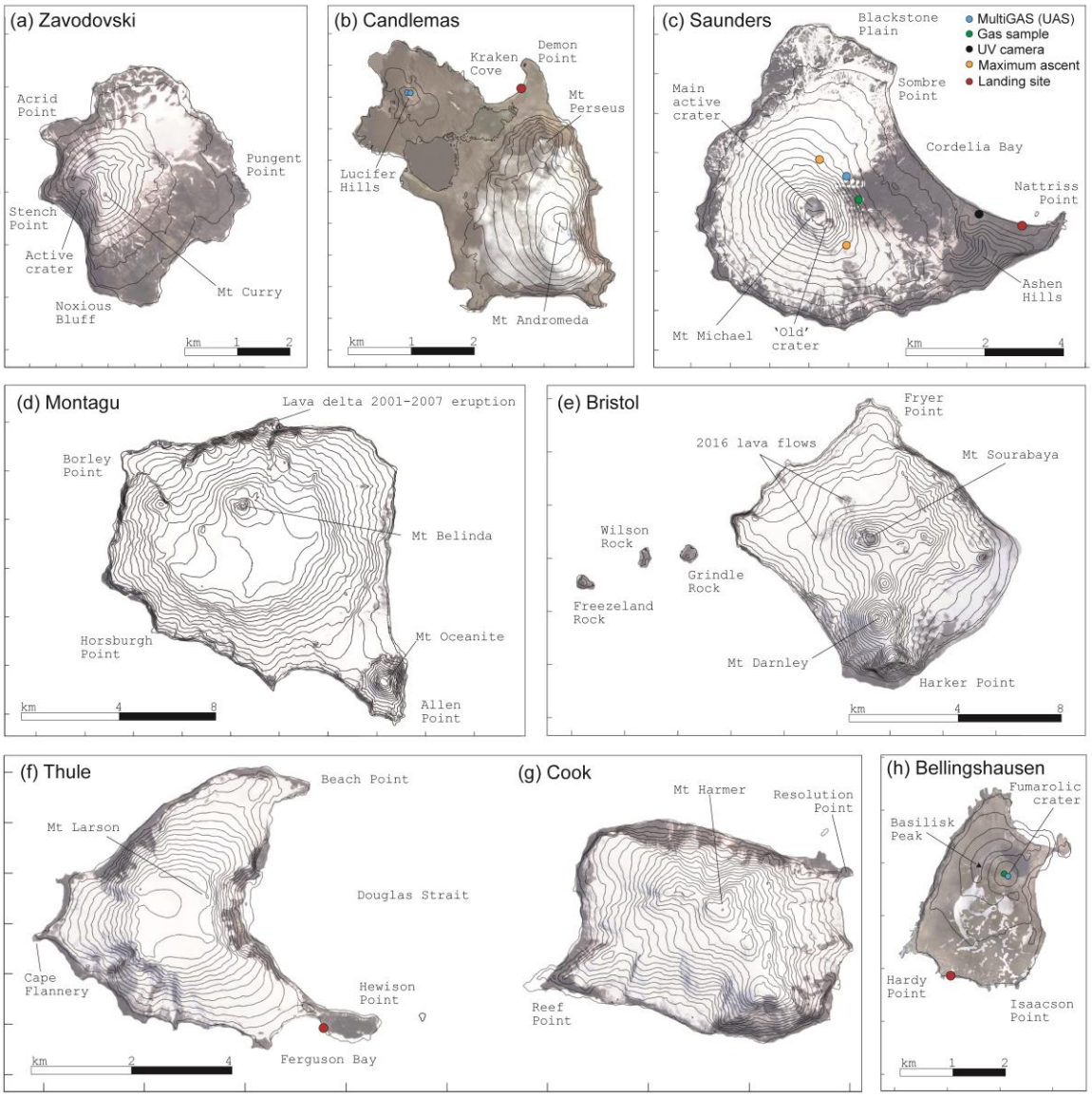

Figure 2: Detailed location maps for the South Sandwich Islands (to scale). Key locations discussed in the main text, such as landing and sampling sites, are annotated with coloured circular symbols according to the legend in (c). Elevation contours at 50 m are extracted from WorldDEM DTM™ (© DLR e.V. 2019 and © Airbus Defence and Space GmbH 2019). Background images are (a–g) Copernicus Sentinel-2 satellite imagery (European Space Agency) acquired on 2 Dec 2019 (Montagu), 5 Dec 2019 (Zavadovski) or 24 Dec 2019 (all others islands); and (h) Orthorectified image generated from Unoccupied Aerial System imagery acquired on 10 Jan 2020 using Agisoft Metashape Professional (version 1.6.3).

METHODS

We report on the state of current volcanic activity along the South Sandwich volcanic arc, with an emphasis on active outgassing. These observations were made during a five-week expedition to South Georgia and the South Sandwich Islands in January 2020 aboard the *Pelagic Australis*. We sailed from Stanley, Falkland Islands, on 30 December 2019 and returned to harbour on 30 January 2020. We made shore landings by zodiac on Saunders Island on three consecutive days between 6 and 8 January; Thule Island on 10 January; Bellingshausen on 11 January; and Candlemas on 12 and 13 January. A landing at Zavodovski was unfortunately not possible due to inclement weather and ocean conditions, but we report visual observations made remotely from the vessel. Aerial images of Zavodovski, Candlemas, Saunders, Bristol, and Bellingshausen were acquired using a small Unoccupied Aerial System (UAS; DJI Mavic 2 Pro). Aerial gas measurements (see instrument specification below) were acquired using a multi-rotor UAS (DJI Matrice 200 modified with custom mounting platform). Full permissions for beyond visual line of sight UAS flights were obtained from the Government of South Georgia and the South Sandwich Islands under Air Navigation (Overseas Territories) Order 2013. Details of all sampling sites—including coordinates, distance from vent, and access description—are presented in Table S1 (supplementary information). All altitudes reported in the text are extracted from the WorldDEM^{TM} topographic model, which has a relative vertical accuracy of 2 m (4 m absolute) in a 12 m x 12 m raster (© DLR e.V. 2019 and © Airbus Defence and Space GmbH 2019).

Fumarole temperatures were measured using a K-type thermocouple that was calibrated immediately prior to the field campaign. Gas compositions were measured using two versions—ground-based and drone-mounted—of a multi-component gas analyser system (Multi-GAS; Aiuppa et al., 2005; Shinohara, 2005). The plume was sampled through two 1 µm particle filters exposed to ambient air, at a pump rate of 1.0 L/min. Concentrations of CO_2, SO_2, and H_2S were logged at 1 Hz. For the ground-based Multi-GAS, SO_2, H_2S, and H_2 electrochemical sensors (3ST/F-TD2G-1A, T3H-TC4E-1A and T3HYT-TE1G-1A, City Technology) were calibrated for 0–200, 0–100 and 0–200 ppmv, respectively, each with an accuracy of ± 2% and a resolution of 0.1 ppmv. A non-dispersive infrared (NDIR) spectrometer (GasCard NG, Edinburgh Instruments) was calibrated for 0–3000 ppmv CO_2 with an accuracy of ± 2% and a resolution of 0.8 ppmv. Pressure (±1 hPa), temperature (±0.5˚C) and relative humidity (±2%) were also measured at 1 Hz (Galltec sensors). For the aerial Multi-GAS, SO_2 and H_2S electrochemical sensors (3ST/F-TD2G-1A and T3H-TC4E-1A, City Technology) were calibrated for 0–200 and 0–50 ppmv, respectively, each with an accuracy of ± 2% and a resolution of 0.1 ppmv. A NDIR spectrometer (Smartgas Modul Premium2, Microsensorik) was calibrated for 0–5000 ppmv CO_2 with an accuracy of ± 2% and a resolution of 1 ppmv. The unit was shielded from radio frequency interference from the UAS transmission system using a foil wrapping. Pressure (±1 hPa), temperature (±0.5˚C) and relative humidity (±3%) were also measured at 1 Hz using a combined sensor module

(Bluedot BME280) exposed to ambient air. Both Multi-GAS instruments were calibrated with standard reference gases at the University of Palermo immediately prior to the field campaign. All sensor data was logged to a micro-SD card. H_2O concentrations were calculated from records of temperature, relative humidity and time-averaged ambient pressure (according to the Arden Buck equations relating the pressure of vapour saturation to temperature for moist air; Buck, 1981). Time series of gas concentrations were post-processed using Ratiocalc software (Tamburello, 2015). Volcanogenic CO_2 and H_2O were resolved from atmospheric background by subtracting the CO_2 and H_2O in ambient air (measured outside the plume where SO_2=0) from the raw CO_2 time series. H_2S concentrations were corrected for the 13% cross-sensitivity of the sensor to SO_2 (determined during calibration with standard reference gases); for example, although the absolute detection limit of the H_2S sensor is 0.1 ppm, the effective detection limit is $0.13 \times SO_2$ ppm.

Molar gas ratios are derived from the gradient of the linear regression in two-species scatterplots, with the exception of H_2O. Uncertainties are reported as the 95% confidence intervals on the regression. The relative humidity sensor reached saturation very quickly during fumarole measurements at Bellingshausen and Candlemas, and therefore derived H_2O concentrations are of lower quality. H_2O/X ratios, where X is the gas species used as the plume marker, were estimated assuming a simple step-change in concentration $\left(\frac{(H2O_{max}-H2O_{background})}{(X_{max}-X_{background})}\right)$. Due to sensor saturation, derived X/H_2O ratios underestimate the true ratio and will be highly uncertain; we estimate a 50% uncertainty on these values to be conservative, although it is difficult to quantify the error explicitly.

The emission rate, or flux, of SO_2 was determined spectroscopically using a dual UV imaging camera developed at University of Palermo and described in Delle Donne et al., (2019, 2017). The instrument, powered by a lithium polymer battery, was equipped with two JAI CM-140GE-UV cameras sensible to UV-radiation and fitted with two distinct band-pass optical filters (both of 10 nm Full Width at Half Maximum) with central wavelengths of 310 (strong SO_2 absorption) and 330 nm (weak SO_2 absorption). A separate computer was used to command and control operations, and to save the acquired images. We deployed the UV camera on Saunders on 8 January 2019, operating (at 0.5 Hz rate) from 13:50 to 16:40 UTC. During this time interval, the plume was dispersing to the east with the prevailing winds. The plume was grounding down the eastern flank, before lifting off and being transported at an altitude of several hundred metres above sea level.

The acquired images (520 × 676 pixels at 10-bit resolution) were post-processed using standard techniques (Delle Donne et al., 2019, 2017; Kern et al., 2015). Sets of co-acquired images were first combined to obtain sequences of "absorbance" images, and then converted into slant column densities (SCD) using calibrations derived from SO_2 reference cells (uncertainty, ±10%). Finally, a time series of integrated column densities (ICD) were obtained for each dataset by integrating the sequences of SCDs images along a cross-section perpendicular to plume transport. Multiplication of the ICA by the plume speed yielded the SO_2 flux time-series. Plume speeds (uncertainty, ±5%) were derived using the

optical flow algorithm of Lucas and Kanade (1981) to track the motion of plume gas fronts in image sequences (Delle Donne et al., 2019, 2017). Light dilution was corrected for using the method of Campion et al., (2015) and found to be negligible. In-plume multiple scattering effects associated with the highly condensed plume are significant and mean that our derived SCDs almost certainly underestimate the true column density; this is not modelled explicitly, however.

Dilute gas samples for carbon isotope measurements were collected in foil bags using a pumped inlet system operating for 90 seconds. Two bag samples were collected in the downwind plume from Mt Michael, Saunders, and a further two from strong fumarolic emissions within the crater on Bellingshausen. A clean ocean air sample was collected several miles off shore from the Falkland Islands, with the boat engine turned off. Gas samples were analysed for their CO_2 concentration and carbon isotope composition (expressed as $\delta^{13}C$ [‰]) by Delta Ray Infrared Isotope Ratio Spectrometer (Fischer and Lopez, 2016; Ilanko et al., 2018) at the University of New Mexico, US.

RESULTS AND DISCUSSION

4.1 Protector Seamounts

Protector Seamounts represent the northernmost volcanic region of the SSVA. A submarine eruption of rhyolite lava took place at Protector Shoal (a shallow cone within 55 m of the sea surface) in 1962. The eruption produced an extensive pumice raft that was encountered by HMS Protector in the vicinity of Zavodovski island soon after (Gass et al., 1963) and as far as New Zealand over the following years (Coombs and Landis, 1966). No observations were made during this expedition.

4.2 Mt Curry, Zavodovski

Zavodovski hosts a single volcanic edifice, Mt Curry (also known as Mt Asphyxia; 557 m asl), surrounded by an extensive lava platform to the east (Fig. 2). Volcanic activity is focused at a steeply-inclined crater on the southwest flank of Mt Curry (Patrick and Smellie, 2013). Vigorous vapour emissions were first reported in 1819 and similar observations have been reported since, notably in 1830 when emplacement of a fresh ‘pumiceous’ lava flow was also documented on the eastern flank (Holdgate and Baker, 1979). Most recently, ash-rich plumes were observed emanating from the main crater between March and June 2016, covering the eastern flanks in fresh dark ash deposits; large bombs were reportedly ejected from the crater (GVP, 2017a).

The broad, low-lying lava platform on the eastern side of the island has undulating topography with deeply-incised water gulleys. Two pyroclastic cones are visible on the lower flanks of Mt Curry, one of which appears to be constructed from two coalesced explosion craters (Fig. 3d). Columnar jointing is exposed at the base of the eastern margins of the lava platform (Fig. 3f). This quasi-hexagonal fracture geometry forms due to thermal contraction of lava driven by conductive cooling, often

associated with water infiltration into fractures (e.g., Lamur et al., 2018; Phillips et al., 2013; Spry, 1962). Here, straight and uniform columnar fractures—colonnade jointing—are present in the dense lower part of the lava flow, suggesting enhanced cooling gradients as the flow entered the sea. The lack of jointing in the overlying rubbly flow unit indicates that the upper part of the flow was insulated to some degree. A thin layer of pyroclastic deposits appears to mantle the top surface of the lava flows in many of the eroded cross-sections.

Intense outgassing was visible on the western side of the island, originating from the main crater (Fig. 3a)—located on the inclined western flank of Mt Curry—and also from fumaroles within the steeply-eroded cliffs below. The base of the crater was obscured by dense, condensed emissions (Video S1, supplementary information), presumably rich in water vapour. The rim of the crater is precipitously thin, with vertical inside walls. The lower left rim of the crater is heavily fractured, and encrusted in yellow sulfurous deposits from the pervasive fumaroles (Fig. 3a). Dispersed fumarolic emissions are visible in the exposed cliffs, and are particularly prevalent at the base of the cliff directly beneath the main crater.

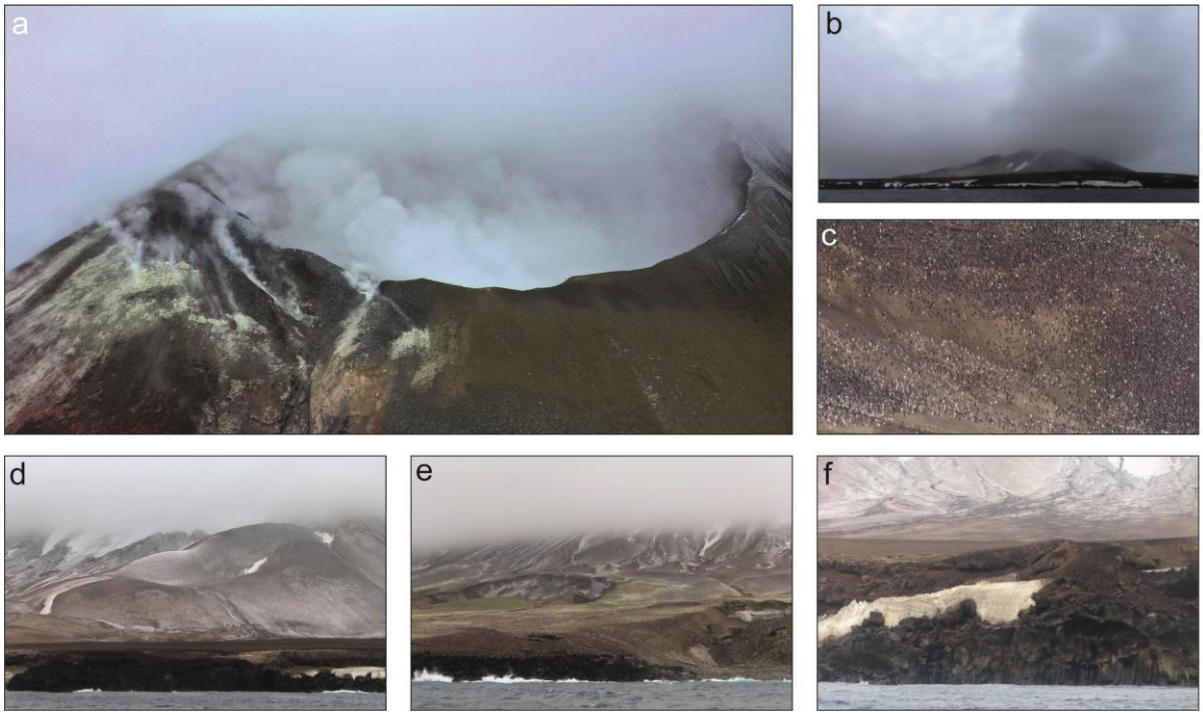

Figure 3: Zavodovski. (a) Persistent gas emissions from the inclined crater on the southwestern flank of Mt Curry. (b) View of the island from the eastern side. (c) Zavodovski is home to the largest penguin colony on Earth (Hart and Convey, 2018). The image shows a small section of the colony; each white/black dot is one of tens of thousands of penguins. (d) Pyroclastic cone on the eastern flank of Mt Curry. (e) Broad lava platform on the eastern side of the island; some parts have been colonised by vegetation. (f) Columnar jointing in the base of the lava flow units exposed on the eastern coast.

The local stratigraphy is well-exposed in the cliffs between Acrid Point and Noxious Bluff, passing Stench Point (Fig. 4; Video S2, supplementary information). The rocks are vibrant shades of red through yellow, indicative of intense oxidative and hydrothermal weathering. At the base of the sequence, a series of relatively thin lava flows are interbedded with thin pyroclastic units. Thick lava flow units with minor pyroclastic intervals characterise the middle part of the stratigraphy. Thick pyroclastic units cap the upper part of the sequence, with a sharp contact with the underlying flow units. Pyroclastic deposits are horizontally-layered and mantle the topography of underlying units. The stratigraphic transition from basal lava flows with minor pyroclastic intervals to dominantly pyroclastic emission suggests a general evolution from effusive cone-building activity to more explosive activity through time. A layered pyroclastic deposit mantles the topography, suggesting deposition as ashfall, and is particularly well-preserved on Stench Point (Fig. 4c, f). Vertical dyke-like structures are visible in the stratigraphy, standing proud by resistance to erosion, however it is unclear where they originate or terminate (Fig. 4b, e). The ubiquitous dense, angular bombs scattered over Stench Point (Video S2, supplementary information) represent ballistic projectiles emitted from the main crater during periods of enhanced explosive activity, most likely in 2016.

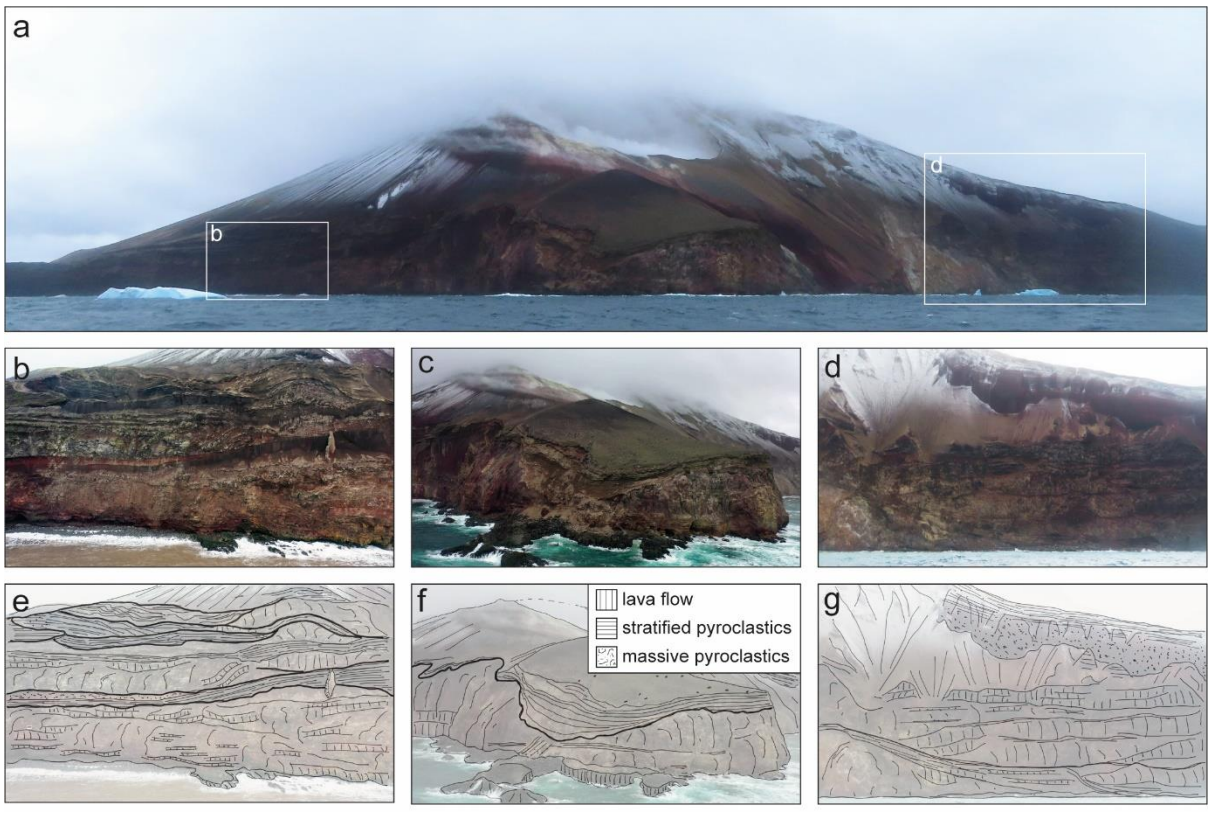

Figure 4: Pyroclastic deposits and lava flows exposed on the west coast of Zavodovski. (a) Overview of the inclined crater and exposed geology. (b–d) Cliffs expose sequences of alternating thick lava flow units and red oxidised pyroclastic deposits. Overlying layered pyroclastic units mantle the topography. (e–f) Annotated sketches of images b–d highlighting stratigraphic relationships.

4.3 Lucifer Hills, Candlemas

Candlemas is dominated by the imposing forms of two steeply-eroded stratovolcanoes, Mt Perseus and Mt Andromeda (557 m asl; Fig. 2), both extensively glaciated. Steep cliffs beneath the ice cap expose a thick stratigraphy of alternating lava flows and pyroclastic units (Fig. 5b). Historically, active volcanism is been focused at the Lucifer Hills Complex, a series of coalesced cinder cones in the northeast region of the island (140 m asl; Fig. 5d–e). Here, andesitic-dacitic extrusive activity has built a radial promontory composed of multiple overlapping lava flow units of unknown age. Dark brown clouds emanating from Lucifer Hills were observed in 1823 and 1911, possibly in association with lava extrusion (LeMasurier et al., 1990). Steam emissions have been repeatedly reported from abundant fumaroles, most recently in 2006 (Patrick and Smellie, 2013). Geothermal activity in the form of geysers and hot pools were reported by LeMasurier et al., (1990) but were no longer visible by 1997. Satellite observations between 2000–2010 detected a persistent thermal anomaly centred on Lucifer Hills (Patrick and Smellie, 2013).

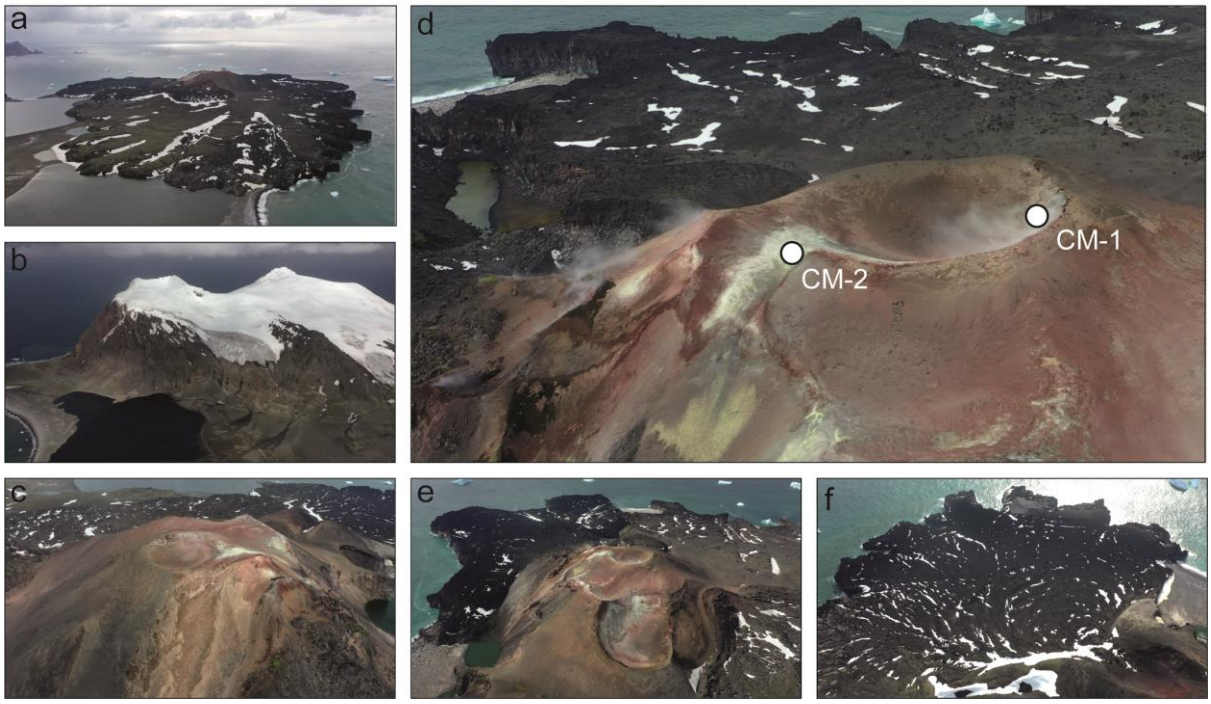

Figure 5: Candlemas. (a) Lucifer Hills Complex and lava peninsula. (b) Glaciated terrain of eroded stratovolcanoes Mt Perseus and Mt Andromeda. (c–e) The overlapping pyroclastic cones of Lucifer Hills, showing pervasive fumarolic outgassing. Gas sampling areas A and B are annotated; coordinates and location details are presented in Table S1, supplementary information. (f) Radiating flow textures on the surface of viscous lava flow lobes.

The peninsula is composed of silicic lava flows (andesite to dacite; Baker, 1978; Pearce et al., 1995) that have built an extension to the main island landmass. The lava flows are arranged in overlapping lobes that protrude out into the sea. The flows originate from small scoria cones within the main Lucifer Hills complex, and can generally be traced back to breaches of the cone wall (Fig. 5f). The flows are generally thick and brecciated, and have not travelled far from their source vents. Aerial views show radiating surface ridges (Fig. 5f) resembling those reported in silicic lava flows at Cordon-Caulle (Farquharson et al., 2015). Surface ridges are compressional features formed in response to flow under a cross-sectional viscosity gradient (between the cooled crust and the hot, fluid lava beneath; Fink, 1980).

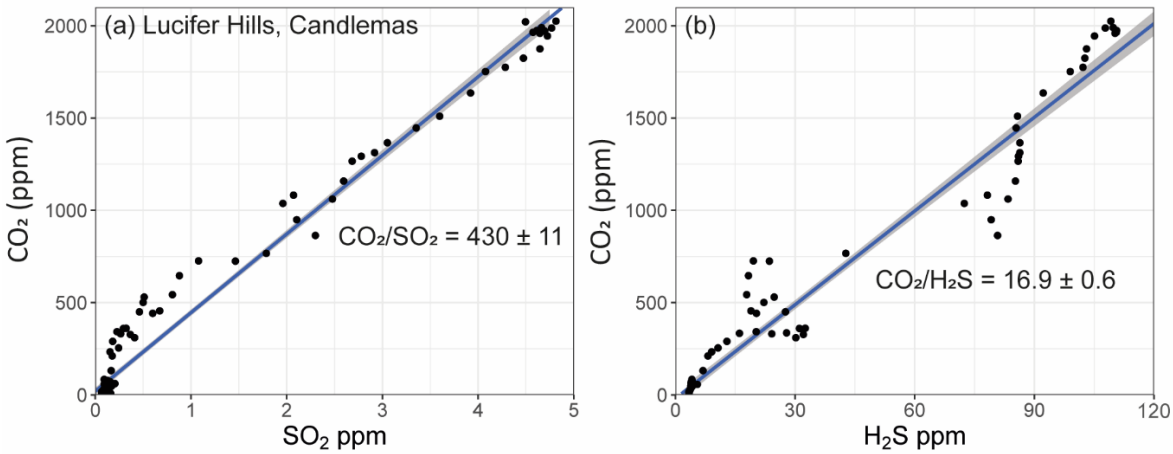

Figure 6: Molar gas ratios sampled at the summit fumaroles at location CM-2 (see Fig. 4d) on Lucifer Hills, Candlemas. CO_2 concentration is reported with atmospheric background subtracted (418 ppm).

Outgassing activity is currently focused around the rim of the summit crater, with a further region of diffuse steaming ground located on the upper western flank of the edifice. We sampled the summit crater emissions in two places: first at a fumarole on the inside of the eastern rim, and then at another on the southwestern rim (annotated on Fig. 5d and described in Table S1, supplementary information). The two measurement sites showed contrasting gas compositions, as measured by multiGAS (Fig. 6; Table 1). We detected substantial excess CO_2 concentrations up to 2134 ppm (after subtraction of an atmospheric background concentration of 407 ppm) at the first fumarole site CM-1, but no sulfur species. Gas temperatures at the point of emission ranged from 88 to 97 °C, but varied by less than 2 °C during repeat measurements at each fumarole. The second fumarole site CM-2, in contrast, was encrusted by conspicuous yellow sulfur deposits and its emissions contained detectable SO_2 and H_2S (in the proportion $H_2S/SO_2 = 25.6 \pm 2.2$), together with excess CO_2 concentrations up to 2027 ppm. Gas temperatures were not measured. We measured a CO_2/SO_2 ratio of 430 ± 11, equivalent to a CO_2/S_T of 16.4 ± 3.3 when combined with H_2S. H_2O was calculated for both sites based on pressure, temperature, and relative humidity (see Methods; Table 1).

Table 1

Molar proportions (%) of gas species present in fumarolic emissions. S_T refers to total sulfur (SO_2 + H_2S). All gas molar ratios are presented in Table S2, supplementary information. H_2O was not calculated for the dilute Mt Michael plume sample. Details of all sampling sites are presented in Table S1, supplementary information. nd = not determined.

Location	ID	T (°C)	H_2O	CO_2	SO_2	H_2S	H_2	CO_2/S_T
Bellingshausen	MG-BH-1	99	88.1 ± 23.5	11.5 ± 2.1	0	0.3 ± 0.05	0.12 ± 0.02	38 ± 2
	MG-BH-2	87	75.4 ± 18.9	24.2 ± 3.9	0	0.2 ± 0.04	0.15 ± 0.02	101 ± 6
Candlemas	MG-CM-1	96	75.7 ± 47.5	25.5 ± 9.6	0	0	0.62 ± 0.24	n/a
	MG-CM-2	nd	63.9 ± 37.9	29.9 ± 9.6	0.1 ± 0.02	1.8 ± 0.57	4.31 ± 1.38	16 ± 7
Mt Michael, Saunders	MG-S-1	ambient						1.8 ± 0.2

4.4 Mt Michael and Ashen Hills, Saunders Island

Saunders is dominated by the conical form of Mt Michael (890 m asl; Fig. 2). There are two active vents at the summit: a main crater ~500 m diameter and a smaller subsidiary ice-filled crater to the southeast that has been visibly emitting gas since 2006 (Patrick and Smellie, 2013) despite having previously been considered inactive (Holdgate and Baker, 1979). The edifice is extensively glaciated and the upper flanks are heavily crevassed. The only ice-free areas are the southeastern peninsula at Nattriss Point, which includes the Ashen Hills pyroclastic cone complex, and the northeastern tip of the island where basaltic lava flows are exposed at Blackstone Plain (Fig. 2). Recurrent thermal anomalies in multi-spectral satellite imagery suggest the presence of a persistent lava lake within the crater (Fig. S1, supplementary information; Gray et al., 2019; Lachlan-Cope et al., 2001). Dual-band processing of these multispectral data yield temperatures of 989–1279 °C, consistent with the expected magmatic temperatures of molten basalt amongst a cooler crust ~200 °C (Gray et al., 2019). Reports of a strong gas plume from the summit of Mt Michael extend back almost continuously to 1820 (LeMasurier et al., 1990). Recent activity includes persistent passive outgassing with sporadic ash-rich explosions (Gray et al., 2019; Patrick and Smellie, 2013). These transient periods of explosive – presumably Strombolian – activity deposit tephra (ash and larger lapilli/bombs) over the eastern flanks of the volcano, reflecting the prevailing wind direction.

Strong and persistent gas emissions emanated from the summit of Mt Michael during 5–8 January 2020. The plume varied from semi-transparent to condensed, and could be traced downwind over the ocean for several tens of kilometres (Fig. 7a, b). On 7 January, we flew the aerial Multi-GAS instrument on-board a multi-rotor UAS (see Methods) from mid-way up the flanks of the volcano to intercept the plume at an altitude ~300 m above ground level (~600 a.s.l). The launch site was ~600 m

382 northeast of the summit vent, and full details of the sampling site and access requirements are presented
383 in Table S2 (supplementary information). Blizzard conditions combined with treacherous crevassed
384 terrain prevented closer ascent to the summit in pursuit of higher gas concentrations. Linear regression
385 of the SO_2 and CO_2 timeseries yield a molar CO_2/SO_2 ratio of 1.8 ± 0.2 (where the uncertainty reported
386 is the standard error of the regression; Fig. 7d). At the dilute plume concentrations encountered (< 1
387 ppm SO_2) and strong eddying winds, there is considerable noise in the data that translates to uncertainty
388 in the gas ratio. We therefore calculated the ratio based on a subsection of the total time series
389 corresponding to the abrupt step-change in gas concentrations observed when the UAS first intercepted
390 the plume (n=72, where sampling rate is 1 Hz), using a background value that represents an average of
391 the preceding 30 seconds of measurements. We recognise that the strength of the correlation is not ideal
392 and so should be interpreted with appropriate caution. H_2S was not present above detection limit (~13%
393 cross-sensitivity to SO_2) in either the aerial or ground-based measurements.
394

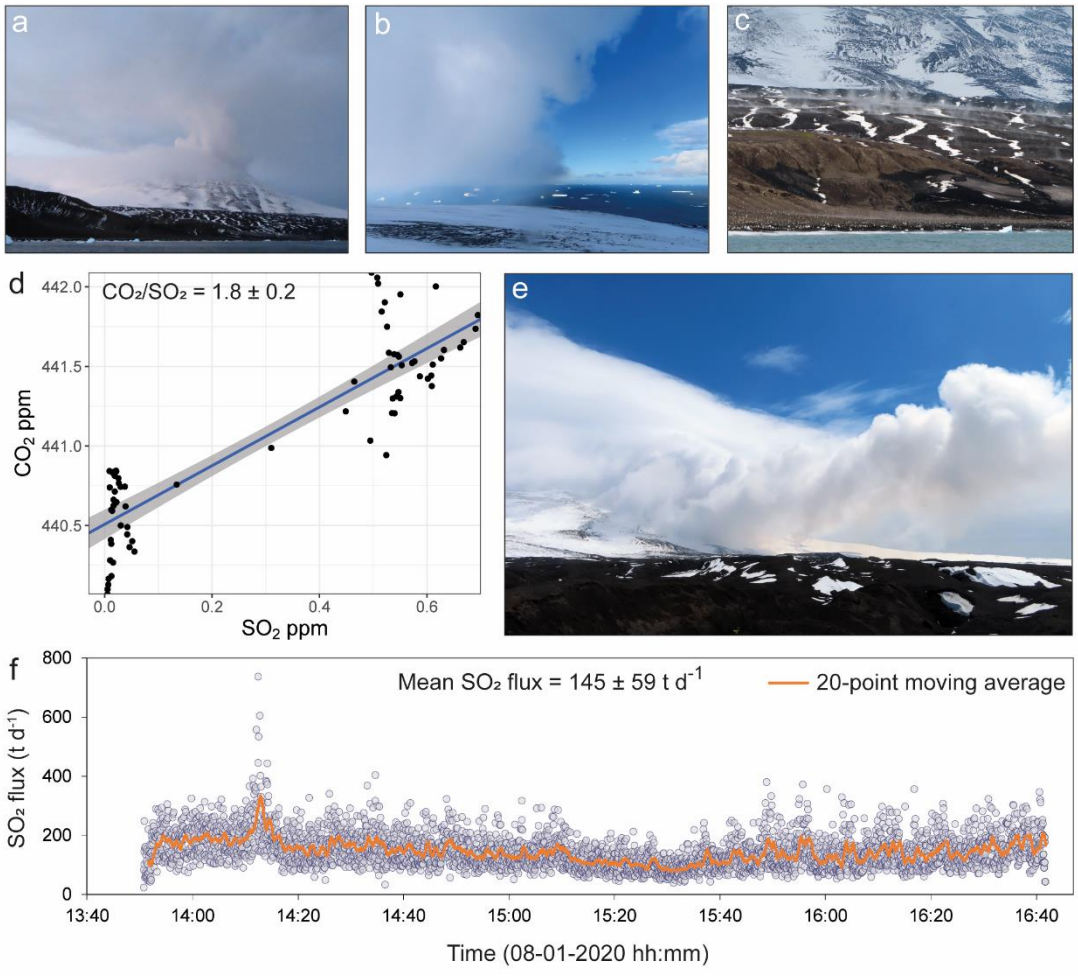

395

396 **Figure 7: Gas emissions from Mt Michael, Saunders Island.** (a) View from the boat of a vertically
397 rising plume on the evening of 5 January 2020. (b) Looking eastwards out to sea on 7 January 2020
398 shows the difference in visibility in and out of the gas plume. (c) Steaming ground, and a ground surface
399 warm to touch, suggests widespread geothermal heating. (d) CO_2-SO_2 scatterplot measured using aerial

multi-GAS on 7 January 2020, showing linear regression. Grey shaded region shows 95% confidence interval. (e) The condensed gas plume from Mt Michael on 8 January 2018, showing the plume travelling at ground level down the eastern flank before lifting off. (f) SO_2 flux timeseries on 8 January 2020. Flux data are calculated from UV camera SO_2 absorbance images multiplied by a plume speed derived from optical flow (see Methods).

Westerly winds on 8 January caused the gas plume to fumigate the eastern flanks of the volcano, yet blizzard conditions and poor-visibility prevailed at the summit. The plume travelled at ground level down the eastern flanks of Mt Michael – resulting in a distinctive blueish haze at ground level – before lifting off over the ocean (Video S3, supplementary material). We encountered SO_2 concentrations up to 2.5 ppm ~600 m downwind on the upper flanks of the volcano (~850 m to the east of the summit vent; Table S2): dilute, but enough to be felt in the nose and throat. CO_2 concentrations during this measurement were affected by radio interference, and so, despite attempted correction using signal processing methods, the dataset was unusable.

We derive an SO_2 flux of 145 ± 59 [σ] t d^{-1} from ~3 hrs of UV camera measurements acquired between 13:40 and 16:40 UTC on 8 January (Fig. 7f; data presented in Table S1 and Fig. S2, supplementary information) approximately perpendicular to the direction of plume transport (camera location annotated on Fig. 2c). Plume and ambient sunlight conditions remained relatively constant during this time interval. The condensed nature of the plume introduces additional uncertainty related to multiple scattering effects and leads us to underestimate the total flux, although we do not model this explicitly.

Stratigraphic sequences of tephra (ash and scoria lapilli) layers are preserved in the glacial ice and exposed in crevasse walls (Fig. S3, supplementary information). A layer of well-sorted coarse scoria lapilli (42 cm thickness) preserved in the upper parts of a crevasse was found to be laterally continuous over tens of metres, and similar but slightly thinner deposits were observed elsewhere. The upper part of this deposit has a distinctive band of red oxidation, suggesting a period of subaerial exposure before snow burial. Given the sharp lower boundary of the deposit against the underlying ice, and the well-sorted nature of the clasts, we propose that this deposit is stratigraphically in-situ and represents a single explosive phase of uncertain duration. Although we lack specific age constraints, given the regional snow accumulation rate we expect this layer to have been deposited within the last five years. The ground surface on the eastern flank is covered by 10–30 cm of loose, unconsolidated ash and lapilli deposits that have likely been remobilised by wind or water. Widespread steaming ground, warm to the touch just below the surface, suggests that geothermal heating is pervasive across the island (Fig. 7c).

Ashen Hills comprises a cluster of overlapping hydromagmatic tuff cones and their associated pyroclastic deposits; the cone complex forms a striking topographic feature of the southeast peninsula of Saunders. Tuff cones (and rings) are built by explosive magma-water interaction involving the

interaction of magma with either ground- or surface water (e.g., Sohn and Chough, 1989; Wohletz and Sheridan, 1983). Bombs of dense lava are widespread (Fig. 8d), suggesting considerable syn-eruptive fragmentation and ejection of country rock material. The ages of the Ashen Hills eruptions are currently unconstrained, as is the geochemical relationship between the Ashen Hills magma and that erupting presently at the summit of Mt Michael.

Fluvial run-off channels in the Ashen Hills expose sequences of stratified tephra deposits several tens of metres thick (Fig. 8). Large-scale sedimentary features include cross-stratification and undulatory bedding that resemble similar features described from 'dry' base surges more generally (e.g., Sohn and Chough, 1989; Waters and Fisher, 1971). Base surges are turbulent, low-particle concentration density currents that are associated with explosive hydromagmatic activity and can be variably water-saturated (Moore, 1967; Nemeth et al., 2006; Waters and Fisher, 1971). Tephra sequences comprise unconsolidated clast-supported beds of ash-coated lapilli and coarse ash alternating with laminated beds of fine to moderately coarse ash. Accretionary lapilli are common, supporting the involvement of magma-water interaction. Beds vary in thickness laterally and erode to produce characteristic circular formations, similar to those observed in eroded base surge deposits elsewhere (e.g., Hverfjall, Iceland; Liu et al., 2017). Unlike many tuff cones, the Ashen Hills deposits are not visibly palagonised.

Figure 8: Ashen Hills pyroclastic cone complex. (a) The pyroclastic deposits are heavily incised by fluvial erosion into regularly-spaced channels. (b, c) Layered deposits with large-scale cross-stratification. (d) Dense bombs are up to metre-scale are widespread; (e) Alternating deposits of fine ash laminations and lapilli beds. Lapilli are generally coated in fine ash, forming coated pellets.

4.5 Montagu

Montagu is a steep-sided eroded stratovolcano (Fig. 2). The structure of the summit region is dominated by a ~6 km-wide ice-filled summit caldera – remnant from pre-historical explosive activity – that hosts an active intra-caldera cone, Mt Belinda (1125 m asl). A prolonged summit eruption from Mt Belinda began in 2001 and continued until 2007, during which eruptive activity included low intensity explosive activity, a persistent steam/ash-plume, and several effusive events (Patrick et al., 2005; Patrick and Smellie, 2013). A particularly voluminous lava flow in 2005 reached the ocean and built up a sizeable lava delta at the point of entry. Prior to this eruption, there has been no documented Holocene activity at Montagu (LeMasurier et al., 1990). Average annual SO_2 emission rates, measured by satellite OMI, declined abruptly from 180 t d^{-1} to < 50 t d^{-1} following the end of the effusive eruption in 2007 (Carn et al., 2017). No observations were made during this expedition.

4.6 Bristol

Bristol has been one of the most frequently active subaerial volcanic centres in the SSI over the last century. Historically, volcanic activity has been focused at Mt Sourabaya (1155 m asl; Fig. 2)), although the highest point of the island is Mt Darnley (1100 m asl). Eruptions are reported from 1935, 1956, 1962 (unconfirmed) and most recently April–July 2016 (GVP, 2017b; Holdgate and Baker, 1979). A summit overflight in 1997 indicated that the summit of Mt Sourabaya is built of three coalesced vents and steaming pyroclastic cones (Patrick and Smellie, 2013). Two substantial lava flows were emplaced concurrently during the 2016 eruption, alongside frequent low intensity ash plumes from the summit cones that were visible in satellite imagery (GVP, 2017b). We did not observe any expressions of active volcanic activity or degassing as we sailed close on January 2020, although the summit was obscured.

Freezeland Rock is the largest of three small islets (inc. Grindle Rock and Wilson Rock) located on a linear trajectory immediately west of Bristol Island (Fig. S4, supplementary information). The edifice is elongated in an E-W direction and constructed from stratified pyroclastic deposits, mainly tuffs and agglomerates, cross-cut by dyke structures of andesitic composition (Holdgate and Baker, 1979). The three islets are considered the remnant deposits of one or more offshore volcanic centres.

4.7 Southern Thule

The islands of Bellingshausen, Cook and Thule are the subaerial exposures of a much larger submarine landform, collectively known as Southern Thule (Fig. 2). Thule and Cook represent the steeply-eroded western and eastern flanks, respectively, of a large submerged caldera (Kemp and Nelson, 1931; Smellie et al., 1998). Cook is extensively glaciated and bounded by steeply-eroded cliffs. Interbedded lavas and

red, oxidised scoriaceous deposits are exposed in the cliff walls, especially at Resolution Point (Fig. 9a, b). There is no record of historical volcanic activity. Thule is entirely glaciated, notably except for an ice-free peninsula at Hewison Point where pyroclastic sequences and dense lavas are exposed (Fig. 9c-e). A 1.5–2 km wide ice-filled caldera is visible at the summit of Mt Larsen (746 m asl), the highest point on Thule (Smellie et al., 1998). Steam was observed emanating from a small intra-caldera summit crater in 1962 (LeMasurier et al., 1990), but no emissions have been reported since (Patrick and Smellie, 2013).

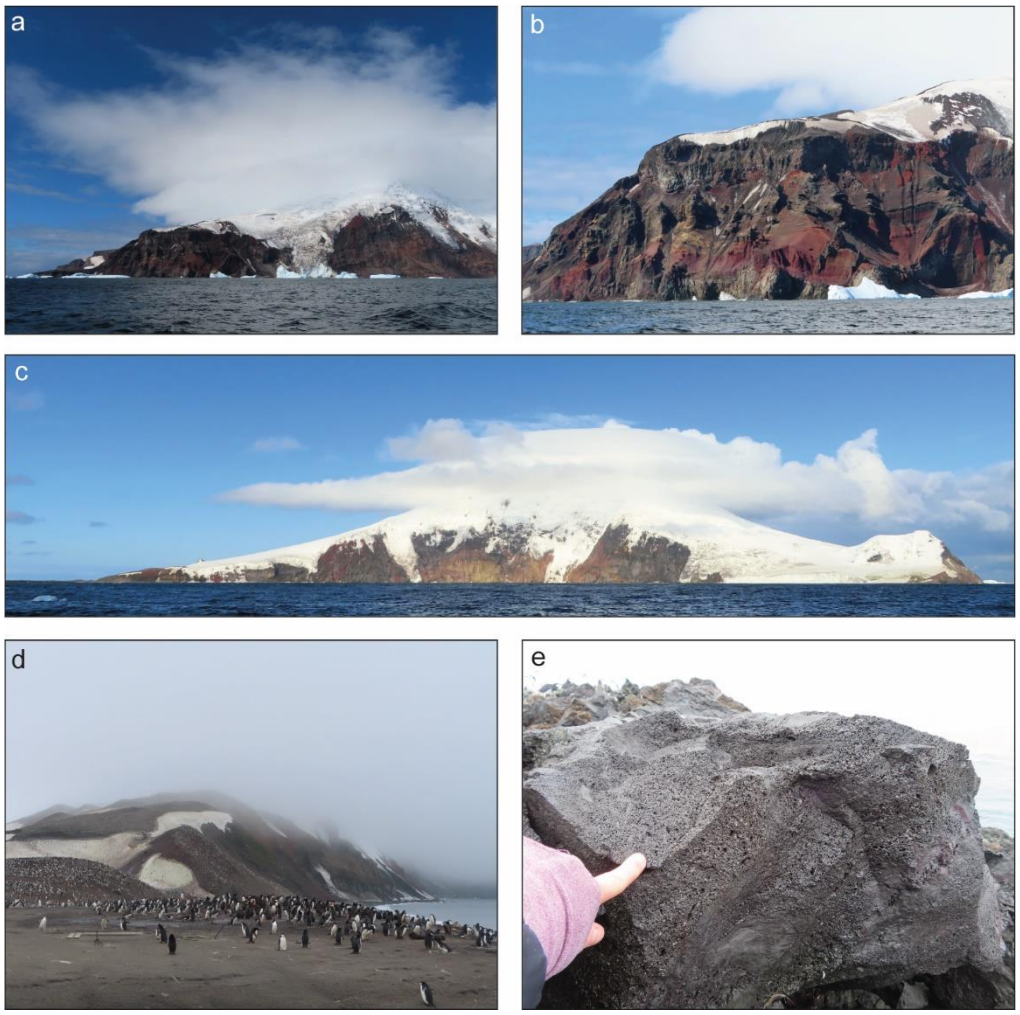

Figure 9: Southern Thule. Cook Island: (a) Exposed lavas and red-oxidised pyroclastic deposits. (b) Resolution Point, on the northeast corner of the island, is one of the most extensive cliff exposures. Thule Island: (c) Overview approaching from the north. (d) View from the ice-free peninsula of Hewison Point towards an oxidised scoria cone on the lower flank of Mt Larsen. (e) Heterogeneously vesicular lavas on Hewison Point.

4.7.1 Bellingshausen

Bellingshausen Island is a small, simply-structured, volcanic cone composed of stratified pyroclastic deposits and lava flows; it is thought to be one of the youngest subaerial islands in the SSI (Holdgate

and Baker, 1979). The highest point of the island is on the western rim of the cone at Basilisk Peak (182 m asl; Fig. 2) and the cone tapers to a broad lava plateau to the south. The margins of the island are deeply incised by coastal erosion, exposing vertical cliffs of layered lava flow units (Fig. 10b). The northeast and eastern flanks of the volcanic cone are truncated by a sector collapses, exposing the internal stratigraphy (Figs. 10, 11). A thick layer of welded agglutinate is found wherever the base of the sequence is exposed, overlain by several hundred metres of decimetre-scale massive lava flows interbedded with stratified pyroclastic layers of ash and scoria that dip away radially away from the cone centre in all directions and resemble fall deposits (Fig. 11). Cross-cutting discontinuities between pyroclastic units suggest multiple phases of fall deposition, each separated by periods of erosion. The sequence is capped by a dense lava flow unit.

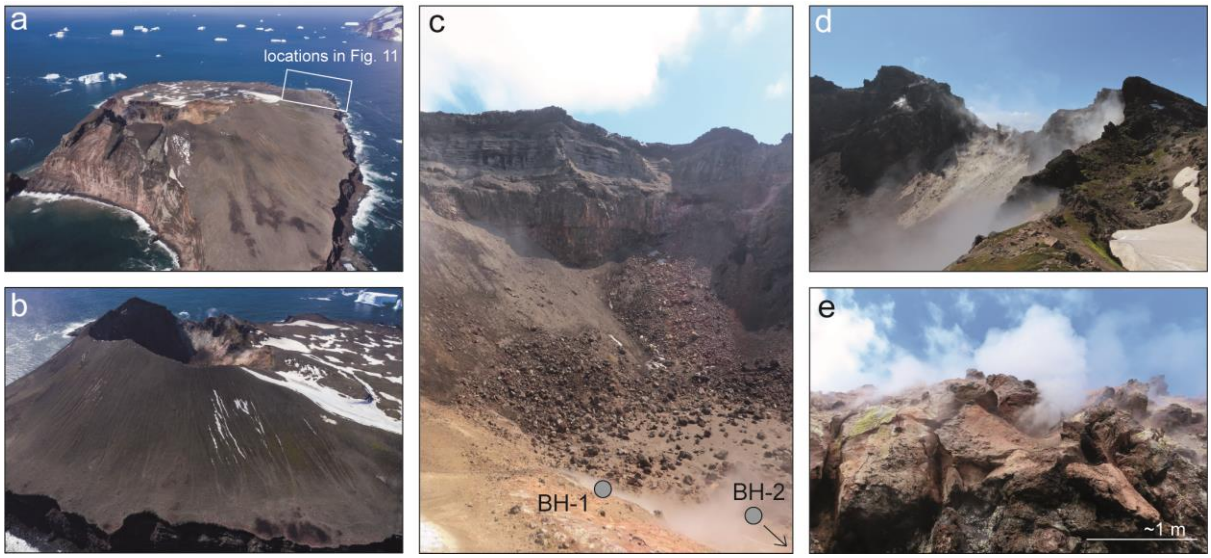

Figure 10: Bellingshausen Island. (a) Aerial image showing the large sector collapse scar on the northern flank of the cone. (b) The cone is bounded by a broad lava platform, with steeply incised wave-cut cliffs. (c) Stratigraphy exposed inside the crater shows thick, massive lava flow units capped by stratified pyroclastics. The fumaroles sampled are visible in the base of the image. (e) Extensive fumarolic outgassing from the western rim of the crater. (f) Audible gas emissions emanating from Fumarole BH-1 at ~99 °C.

Fumarolic outgassing inside the crater and along the seaward side of the eastern crater rim was reported by Holdgate and Baker (1979) and again in 1997, together with low temperature thermal anomalies in satellite imagery between 2000 and 2010 (Patrick and Smellie, 2013). We observed a similar distribution of emissions sources from numerous fumarolic areas on the walls and base of the crater; together with ubiquitous diffuse emissions from the hydrothermally-altered clay substrate. These diffuse emissions were composed only of water vapour as no CO_2 or sulfur species were detected by the MultiGAS. We measured and sampled two fumaroles in the centre of the base of the crater, which contributed the densest point source emissions (partially shown in Fig. 10c; full details of the sampling

sites and access requirements are presented in Table S2, supplementary information). Gas temperatures range from 96 to 98°C. The gas composition as measured by MultiGAS is dominated by H_2O (75–84 mol%) and CO_2 (12–24 mol%), with minor H_2S (0.2–0.3 mol%) and H_2 (<0.2 mol%; Table 1). No SO_2 was present above the detection limit of 0.1 ppm. CO_2 and H_2S exhibit strong positive correlation ($r^2 > 0.99$), with distinct gradients for the two different fumaroles (Fig. 12). CO_2/S_T ratios (where S_T refers to total sulfur) range from 40.6 ± 2.1 at the strong and audibly degassing fumarole BH-1 (gas temperature 99°C; Fig. 10f) to 100.1 ± 5.7 in a region of more diffuse and non-audible emissions downwind from multiple distributed gas sources (fumarole BH-2), about 10 m away from fumarole BH-1 (Fig. 12).

Thick lava flow units of basaltic andesite composition (Leat et al., 2003) dominate the stratigraphy in the south of the island. Layered pyroclastic fall deposits of ash/fine lapilli are exposed on the southwest tip of the island at Hardy Point, however (Fig. 11a). Where the lava flows are exposed on the beaches at Hardy and Isaacson Points, they exhibit a bulbous, brecciated structure with curved brittle fracture surfaces (Fig. 11d–f). The interiors of the flows are moderately-vesicular with elongated tear-shaped vesicles.

Figure 11: Tephra deposits and lava flows, Bellingshausen Island. (a) Stratified pyroclastic fall deposits (ash/lapilli) on the peninsula of Hardy Point. (b) Jagged Point, erosion has revealed a base of welded agglutinate overlain by stratified pyroclastic deposits. (c) Annotated sketch highlighting the main stratigraphic relationships. (d–e) Lava flow textures exposed in the basaltic andesite flows at Hardy Point.

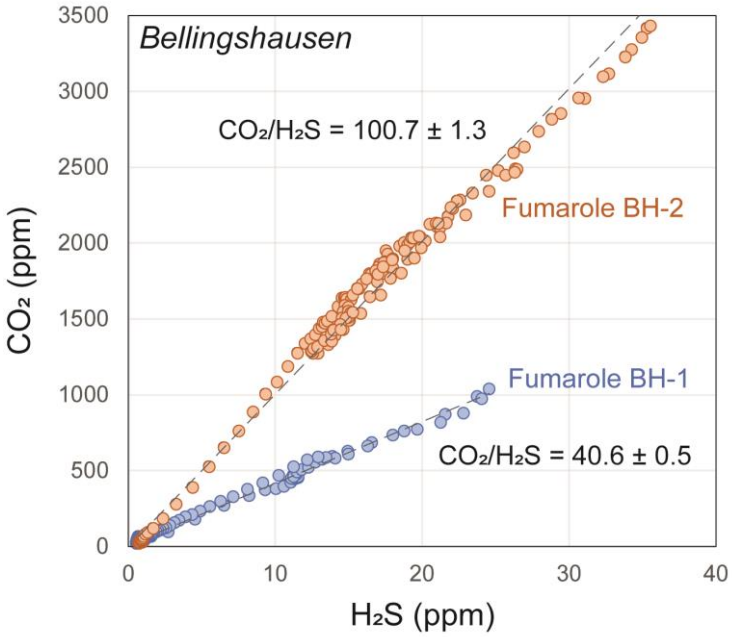

559

560 **Figure 12:** Molar gas ratios from fumaroles sampled in the centre of the crater on Bellingshausen.
561 Fumarole BH-1 is partially visible in the base of the image in Figure 10c. CO_2 concentration is reported
562 with atmospheric background subtracted (419 ppm).

563

564 **4.8 Volcanic gas compositions (CO_2/S) and SO_2 flux**

565 Molar CO_2/S_T gas ratios from the SSVA vary between 1.8 and 101, reflecting variable interaction of
566 magmatic fluids with hydrothermal systems. Scrubbing of sulfur species by gas-rock-water reactions
567 under hydrothermal conditions—especially at weak, low temperature fumaroles (<250 °C)—produce
568 highly variable CO_2/S_T ratios in fumarolic emissions that vary over several orders of magnitude
569 (Giggenbach, 1996; Symonds et al., 2001). Di Napoli et al. (2016) simulate the influence of scrubbing
570 on gas chemistry at near surface conditions, producing a model that reproduce the near-exponential
571 decrease in CO_2/S_T with increasing temperature observed in global compilations of volcanic gas
572 measurements (Fig. S5, supplementary information; Aiuppa et al., 2017 and references therein). Low
573 temperature fumarolic emissions measured at Bellingshausen and Candlemas (T~100 °C; Fig. S5,
574 supplementary information) are characterised by CO_2/S_T ratios that are elevated compared to the range
575 of values associated with high temperature magmatic gases globally (0.2–14.7; Aiuppa et al., 2017). A
576 difference in gas temperature from 99 °C (strong, audible vent) to 87 °C (weaker emission) between
577 two closely-spaced fumaroles within Bellingshausen crater manifests as an increase in the CO_2/S_T ratio
578 from 38 ± 2 to 101 ± 6, respectively (Table 1). Further, H_2S is the dominant sulfur species in the
579 emissions from Candlemas and Bellingshausen, with SO_2 only detected one of the four fumaroles
580 measured. SO_2 is the more prevalent sulfur species in high temperature magmatic gases, being
581 thermodynamically favourable under oxidising conditions, reducing pressures and increasing

temperatures (Gerlach and Nordlie, 1975; Giggenbach, 1996; Moretti and Papale, 2004). Low SO_2/H_2S ratios (i.e., a change in speciation to favour H_2S) reflect chemical equilibration of magmatic gases with colder, more reducing hydrothermal conditions. In the context of interpreting fundamental insights in volatile sources in the SSVA, these low temperature fumaroles provide little insight, as any magmatic signature has been long since overprinted by hydrothermal processes. Monitoring changes in the gas ratios—particularly SO_2/H_2S—would be informative in a hazard context to identify changes in the balance of magmatic and hydrothermal contributions that may precede future phreatic or magmatic activity (e.g., de Moor et al., 2019), but the logistical effort required to sustain such measurements in these remote sub-polar environments would be immense.

Mt Michael is an open vent volcano emitting a modest gas flux of 145 ± 59 t d^{-1} SO_2 from large a summit crater. We measured a molar CO_2/S_T gas ratio of 1.8 ± 0.2 in the downwind plume, which lies close to the median arc composition of ~2 (Shinohara, 2013) or 1.6 (Aiuppa et al., 2017) based on high temperature emissions. Together with the lack of detectable H_2S, this low CO_2/S_T is consistent with a magmatic gas source unmodified by hydrothermal reactions. Globally, the CO_2/S_T is well correlated with the carbon content of the subducted sediments (Aiuppa et al., 2017). Our data from Mt Michael support predicted CO_2/S_T ratios of ~1.2 for the South Sandwich arc based on Ba/La trace element proxies and the carbon-poor nature of regional sediments (Plank, 2005; Aiuppa et al., 2019). Considering total volatile fluxes, our calculated SO_2 flux is of a similar order of magnitude to the time-averaged decadal SO_2 flux of 263 ± 63 [σ] t d^{-1} from the Ozone Monitoring Instrument (OMI) satellite measurements (2005–2015; Carn et al., 2017). Combining the CO_2/SO_2 molar ratio with our independent SO_2 emission rate measured near-simultaneously, we derive a CO_2 flux of 267 ± 112 t d^{-1}. If our CO_2/SO_2 data are representative of the persistent outgassing behaviour of Mt Michael, extrapolating our daily CO_2 emission rate yields an annual carbon output of 0.1 Mt CO_2. However, we emphasise that we present here only a snapshot of the gas chemistry; further measurements at both Mt Michael and Mt Curry (Zavodovski)—the two most strongly degassing volcanoes of the SSI at present— would help to constrain both along-arc and temporal variability in gas chemistry and flux.

4.9 Carbon isotope composition

Fumarole gases and dilute plume emissions from two locations along the SSVA (the dilute summit plume from Mt. Michael, Saunders Island and the fumarole in Bellingshausen crater) populate a linear mixing line from clean ocean air background towards that of the volcanic CO_2 composition (Fig. 12; Table S2, supplementary information). All gas samples have CO_2 concentrations in excess of ambient air (419 ppm) between 467 and 789 ppm, with $\delta^{13}C$ values between -7.8 and -11.3 ‰. Although unconstrained at higher CO_2 concentrations, extrapolation of the mixing line to 100% volcanic CO_2 indicates a $\delta^{13}C$ composition of -4.5 ± 2.0 ‰ (Fig. 14; where $\delta^{13}C$ is the deviation of the ratio $^{13}C/^{12}C$ relative to that of Pee Dee belemnite and the reported error is the standard error of the regression). We

note that our clean ocean air background sample is isotopically light ($\delta^{13}C$ = -10 ‰) compared to the global average suggesting that it may have been fractionated to lighter values during collection. If this is the case, given that all samples were collected and stored in the same way, we assume that all would be fractionated equally. If we normalise our background to the global average $\delta^{13}C$ = -8.5 ‰ (Fischer and Lopez, 2016 and references therein), and apply this offset to all samples, then the extrapolated magmatic carbon isotope composition shifts to a slightly heavier value of -2.9 ± 2.0 ‰.

The two sets of plume and fumarole samples were collected from different positions along the arc: Saunders in the central arc, and Bellingshausen in the southern arc. That all samples populate a single linear trend (regardless of any vertical offset) suggests a common carbon source. From these data—albeit from a small sample size—we propose no fundamental along-arc variation in the carbon isotope composition along the SSVA. Variations within 4 ‰ are indistinguishable given the uncertainties of our dataset and the ambient air regression; more samples with higher concentration CO_2 contents would improve these constraints.

Our best extrapolated value of $\delta^{13}C$ = -4.5 ± 2.0 ‰ (or similarly the background-normalised value of -2.9 ‰) lies at the upper range of the isotopic signature of depleted upper mantle ($\delta^{13}C$ = -6.5 ± 2.5 ‰; Sano and Marty, 1995), and well below the signature of marine limestones ($\delta^{13}C \approx 0$ ‰; Fig. 12). Interpreted most simply, this result suggests that most of the emitted carbon is derived from the mantle wedge with only minor addition of a subducted component. However, Th-Sm-La trace element systematics in SSI arc lavas populate a mixing array between depleted mantle and subducted sediment end-members, indicating a variable (but non-negligible) subduction contribution; the Th-REE compositions of Saunders lavas are consistent with ~50 % sediment and ~50 % mantle, for example (Plank, 2014, 2005; Fig. S6, supplementary information). In ODP 701, carbonate and organic carbon comprise 75% and 25% of the total carbon by mass, although each are distributed differently through the core. Carbonate is concentrated in the lowermost units of the core (~70 m), with the bulk composition reaching 70–90 % $CaCO_3$ in the basal indurated chalk. Organic carbon, in contrast, is evenly distributed at low concentrations ~0.5 wt % throughout the section, apart from a thin carbon-rich ooze at 150 m depth (Ciesielski et al, 1988). If we assign each age-specific $\delta^{13}C$ signatures to these proportions of carbonate and organic carbon (from Hayes et al., 1999), we derive an approximate weighted average $\delta^{13}C$ signature for the sediment pile of -4.8 ‰ (Table S3, supplementary information). Assuming the lithologies exposed in ODP 701 are representative of those entering the South Sandwich trench, this sedimentary carbon contribution would be indistinguishable from depleted mantle using carbon isotopes alone.

Boron isotope enrichments in SSVA lavas point to an additional subduction contribution from altered oceanic crust (Tonarini et al., 2011). Similarly, Th-Sm-La (Plank, 2005) are modelled more effectively by three-component mixing between depleted mantle, sediment, and altered oceanic crust (Fig. S6, supplementary information) as are other trace elements (Pearce et al., 1995). Indeed, subduction of carbonated (serpentinised) peridotite—derived either from the down-going oceanic crust

or eroded forearc—is consistent with the composition of local dredge samples and those from other slow- to ultra-slow spreading settings globally (Lawver and Dick, 1983; Plank and Manning, 2019; Tonarini et al., 2011; Vanneste and Larter, 2002). Globally, the carbon isotope signatures of serpentinites exposed in ophiolite sequences and at oceanic ridges are highly variable—reflecting mixing between seawater carbonate and organic carbon—with bulk $\delta^{13}C$ values ranging from -4.6 ± 5.1 ‰ in the Northern Appenines ophiolites to -13.7 ± 9.6 ‰ in the Lost City hydrothermal field (Alt et al., 2013). From the data presented in this study we cannot evaluate quantitatively the relative contributions from each of the proposed carbon sources. Rather, we intend this discussion to highlight the contrasting scenarios in which both simple and complex mixing of distinct carbon sources may generate the carbon isotopic signature observed in volcanic gas emissions, and thus motivate further research into the efficiency of volatile and trace element transfer through this young arc system.

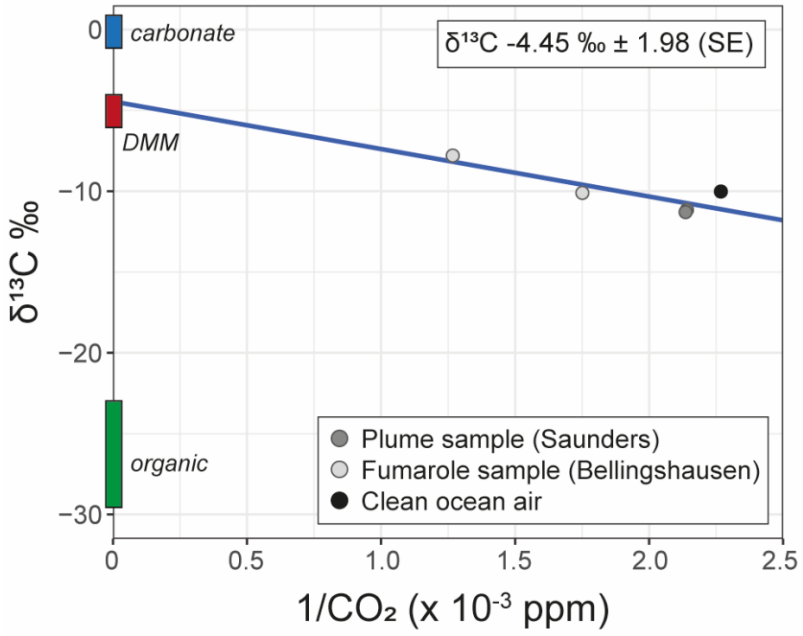

Figure 13: Carbon isotope composition of volcanic gas emissions. Samples include fumarole gases (Bellingshausen), dilute plume emissions (Saunders), and clean ocean air background (at sea). All data points are included in the regression. The intersection of the regression line with the y-axis represents the magmatic carbon isotope composition extrapolated to 100% CO_2. Data presented in Table S2 (supplementary material).

CONCLUSIONS

We present detailed observations from an expedition to the South Sandwich volcanic arc in January 2020 that describe a rich and varied geological history, and we report the first in situ measurements of volcanic gas chemistry, isotopic composition, and emission rate. We show that Mt Michael on Saunders

Island is a persistent gas source, releasing 145 ± 59 t d^{-1} SO_2 and 267 ± 112 t d^{-1} CO_2 in a strong plume characterised by a low CO_2/SO_2 ratio of 1.8 ± 0.2, consistent with input of carbon-poor sediment to the subduction zone. Extrapolating from our measured daily emission rate, the carbon flux from Mt Michael into the atmosphere is ~0.1 Mt CO_2 yr^{-1}. Although our measured SO_2 flux is of a similar magnitude to that of long-term satellite observations between 2005 and 2015 (Carn et al., 2017), temporal variability in gas chemistry is too poorly-constrained at this volcano to speculate on the longer-term carbon flux. Fumarolic outgassing is pervasive in the active centres of Candlemas and Bellingshausen, characterised by carbon-rich and sulfur-poor emissions from low temperature (90–100°C) fumaroles. Strong steam emissions emanate from the crater of Mt Curry, Zavodovski. Carbon isotope measurements of dilute plume and fumarole gases from along the arc suggest a magmatic $\delta^{13}C$ composition of -4.5 ± 2.0 ‰. Considering the potential carbon sources, this carbon isotope signature suggests a dominant contribution from mantle carbon, though mixing between mantle carbon and a subduction component composed of sediment and altered crust is also permissible and more consistent with other geochemical features of South Sandwich magmas. The South Sandwich Volcanic Arc (SSVA) has huge potential for future petrological and volcanological research. It represents an ideal tectonic setting in which to explore the geochemical processes of an exceptionally young arc.

ACKNOWLEDGEMENTS

We are grateful to the crew of the *Pelagic Australis*—Chris Kobusch, Sophie O'Neill, Thomas Geipel—without whom this fieldwork would never have been possible. We also wish a huge thank you to all other expedition members – Paul Mayewski, Mario Potocki, Gemma Clucas, Jo Feldman, Ruth Peacey, Hamza Yassin, and Ted Cheeseman – for their unwavering support in the field and for their sense of humour aboard a small boat for five weeks. In particular, we thank Skip Novak—expedition lead—who assisted us ashore on all our sampling excursions. We acknowledge support from the Government of South Georgia and the South Sandwich Islands This expedition was funded by public donations raised by Quark Expeditions Ltd, by the Government of South Georgia and the South Sandwich Islands (GSGSSI), and by individual contributions. This work was carried out under RAP 2019/025 issued by GSGSSI. EJL was supported by a Leverhulme Early Career Fellowship. A.A. and M.B. acknowledge funding from Miur (Grant N. 2017LMNLAW).

REFERENCES

Aiuppa, A., Federico, C., Giudice, G., Gurrieri, S., 2005. Chemical mapping of a fumarolic field: La Fossa Crater, Vulcano Island (Aeolian Islands, Italy). Geophysical Research Letters 32. https://doi.org/10.1029/2005GL023207

Aiuppa, A., Fischer, T.P., Plank, T., Bani, P., 2019. CO2 flux emissions from the Earth's most actively degassing volcanoes, 2005–2015. Sci Rep 9, 5442. https://doi.org/10.1038/s41598-019-41901-y

Aiuppa, A., Fischer, T.P., Plank, T., Robidoux, P., Di Napoli, R., 2017. Along-arc, inter-arc and arc-to-arc variations in volcanic gas CO2/ST ratios reveal dual source of carbon in arc volcanism. Earth-Science Reviews 168, 24–47. https://doi.org/10.1016/j.earscirev.2017.03.005

Alt, J.C., Schwarzenbach, E.M., Früh-Green, G.L., Shanks, W.C., Bernasconi, S.M., Garrido, C.J., Crispini, L., Gaggero, L., Padrón-Navarta, J.A., Marchesi, C., 2013. The role of serpentinites in cycling of carbon and sulfur: Seafloor serpentinization and subduction metamorphism. Lithos, Serpentinites from mid-oceanic ridges to subduction 178, 40–54. https://doi.org/10.1016/j.lithos.2012.12.006

Baker, 1978. Baker, P.E., 1978. The South Sandwich Islands: iii. petrology of the volcanic rocks (Vol. 93). British Antarctic Survey.

Barker, P.F., 1995. Tectonic Framework of the East Scotia Sea, in: Taylor, B. (Ed.), Backarc Basins: Tectonics and Magmatism. Springer US, Boston, MA, pp. 281–314. https://doi.org/10.1007/978-1-4615-1843-3_7

Barker, P.F., 1970. Plate Tectonics of the Scotia Sea Region. Nature 228, 1293–1296. https://doi.org/10.1038/2281293a0

Basile, I., Petit, J.R., Touron, S., Grousset, F.E., Barkov, N., 2001. Volcanic layers in Antarctic (Vostok) ice cores: Source identification and atmospheric implications. Journal of Geophysical Research: Atmospheres 106, 31915–31931. https://doi.org/10.1029/2000JD000102

Boschen, R.E., Rowden, A.A., Clark, M.R., Gardner, J.P.A., 2013. Mining of deep-sea seafloor massive sulfides: A review of the deposits, their benthic communities, impacts from mining, regulatory frameworks and management strategies. Ocean & Coastal Management 84, 54–67. https://doi.org/10.1016/j.ocecoaman.2013.07.005

Brett, C.P., 1977. Seismicity of the South Sandwich Islands region. Geophysical Journal of the Royal Astronomical Society 51, 453–464. https://doi.org/10.1111/j.1365-246X.1977.tb06928.x

Buck, A.L., 1981. New Equations for Computing Vapor Pressure and Enhancement Factor. J. Appl. Meteor. 20, 1527–1532.

Calvert, A.J., 2011. The Seismic Structure of Island Arc Crust, in: Brown, D., Ryan, P.D. (Eds.), Arc-Continent Collision, Frontiers in Earth Sciences. Springer, Berlin, Heidelberg, pp. 87–119. https://doi.org/10.1007/978-3-540-88558-0_4

Campion, R., Delgado-Granados, H., Mori, T., 2015. Image-based correction of the light dilution effect for SO2 camera measurements. Journal of Volcanology and Geothermal Research 300, 48–57.

Carn, S., Fioletov, V., McLinden, C., Li, C., Krotkov, N., 2017. A decade of global volcanic SO 2 emissions measured from space. Scientific reports 7, 44095.

Ciesielski et al, 1988. Ciesielski, P.F., Kristoffersen, Y., et al., 1988. Proc. ODP, Init. Repts., 114: College Station, TX (Ocean Drilling Program). doi:10.2973/odp.proc.ir.114.1988.

Convey, P., Smith, R.I.L., Hodgson, D.A., Peat, H.J., 2000. The flora of the South Sandwich Islands, with particular reference to the influence of geothermal heating. Journal of Biogeography 27, 1279–1295. https://doi.org/10.1046/j.1365-2699.2000.00512.x

Coombs and Landis, 1966. Coombs, D.S. and Landis, C.A., 1966. Pumice from the south sandwich eruption of march 1962 reaches New Zealand. Nature, 209(5020), pp.289-290.

de Moor, J.M., Stix, J., Avard, G., Muller, C., Corrales, E., Diaz, J.A., Alan, A., Brenes, J., Pacheco, J., Aiuppa, A., Fischer, T.P., 2019. Insights on Hydrothermal-Magmatic Interactions and Eruptive Processes at Poás Volcano (Costa Rica) From High-Frequency Gas Monitoring and Drone Measurements. Geophysical Research Letters 46, 1293–1302. https://doi.org/10.1029/2018GL080301

Delle Donne, D., Aiuppa, A., Bitetto, M., D'Aleo, R., Coltelli, M., Coppola, D., Pecora, E., Ripepe, M., Tamburello, G., 2019. Changes in SO2 Flux Regime at Mt. Etna Captured by Automatically Processed Ultraviolet Camera Data. Remote Sensing 11, 1201. https://doi.org/10.3390/rs11101201

Delle Donne, D., Tamburello, G., Aiuppa, A., Bitetto, M., Lacanna, G., D'Aleo, R., Ripepe, M., 2017. Exploring the explosive-effusive transition using permanent ultraviolet cameras. Journal of Geophysical Research: Solid Earth 122, 4377–4394. https://doi.org/10.1002/2017JB014027

Derrien et al, 2019. Derrien, Allan; Richter, Nicole; Meschede, Martin; Walter, Thomas (2019): Optical DSLR camera- and UAV footage of the remote Mount Michael Volcano, Saunders Island (South Sandwich Islands), acquired in May 2019. GFZ Data Services. http://doi.org/10.5880/GFZ.2.1.2019.003.

Di Napoli, R., Aiuppa, A., Bergsson, B., Ilyinskaya, E., Pfeffer, M.A., Guðjónsdóttir, S.R., Valenza, M., 2016. Reaction path models of magmatic gas scrubbing. Chemical Geology 420, 251–269. https://doi.org/10.1016/j.chemgeo.2015.11.024

Farquharson, J.I., James, M.R., Tuffen, H., 2015. Examining rhyolite lava flow dynamics through photo-based 3D reconstructions of the 2011–2012 lava flowfield at Cordón-Caulle, Chile. Journal of Volcanology and Geothermal Research 304, 336–348. https://doi.org/10.1016/j.jvolgeores.2015.09.004

Fink, J., 1980. Surface folding and viscosity of rhyolite flows. Geology 8, 250–254. https://doi.org/10.1130/0091-7613(1980)8<250:SFAVOR>2.0.CO;2

Fischer, T.P., Lopez, T.M., 2016. First airborne samples of a volcanic plume for δ13C of CO2 determinations. Geophysical Research Letters 43, 3272–3279.

Garabato, A.C., Heywood, K.J., Stevens, D.P., 2002. Modification and pathways of Southern Ocean Deep Waters in the Scotia Sea. Deep Sea Research Part I: Oceanographic Research Papers 49, 681–705. https://doi.org/10.1016/S0967-0637(01)00071-1

Gass, I.G., Harris, P.G., Holdgate, M.W., 1963. Pumice Eruption in the Area of the South Sandwich Islands. Geol. Mag. 100, 321–330. https://doi.org/10.1017/S0016756800056053

Gerlach, T.M., Nordlie, B.E., 1975. The C-O-H-S gaseous system; Part I, Composition limits and trends in basaltic cases. Am J Sci 275, 353–376. https://doi.org/10.2475/ajs.275.4.353

Giggenbach, W.F., 1996. Chemical Composition of Volcanic Gases, in: Scarpa, R., Tilling, R.I. (Eds.), Monitoring and Mitigation of Volcano Hazards. Springer, Berlin, Heidelberg, pp. 221–256. https://doi.org/10.1007/978-3-642-80087-0_7

Giner-Robles, J.L., Pérez-López, R., Rodríguez-Pascua, M.A., Martínez-Díaz, J.J., González-Casado, J.M., 2009. Present-day strain field on the South American slab underneath the Sandwich Plate (Southern Atlantic Ocean): a kinematic model. Geological Society, London, Special Publications 328, 155–167. https://doi.org/10.1144/SP328.6

Gray, D.M., Burton-Johnson, A., Fretwell, P.T., 2019. Evidence for a lava lake on Mt. Michael volcano, Saunders Island (South Sandwich Islands) from Landsat, Sentinel-2 and ASTER satellite imagery. Journal of Volcanology and Geothermal Research 379, 60–71. https://doi.org/10.1016/j.jvolgeores.2019.05.002

GVP, 2017a. Global Volcanism Program, 2017. Report on Zavodovski (United Kingdom) (Crafford, A.E., and Venzke, E., eds.). Bulletin of the Global Volcanism Network, 42:2. Smithsonian Institution. https://doi.org/10.5479/si.GVP.BGVN201702-390130.

GVP, 2017b. Global Volcanism Program, 2017. Report on Bristol Island (United Kingdom) (Crafford, A.E., and Venzke, E., eds.). Bulletin of the Global Volcanism Network, 42:9. Smithsonian Institution. https://doi.org/10.5479/si.GVP.BGVN201709-390080.

Hart, T., Convey, P., 2018. The South Sandwich Islands – a community of meta-populations across all trophic levels. Biodiversity 19, 20–33. https://doi.org/10.1080/14888386.2018.1464952

Hayes, J.M., Strauss, H., Kaufman, A.J., 1999. The abundance of 13C in marine organic matter and isotopic fractionation in the global biogeochemical cycle of carbon during the past 800 Ma. Chemical Geology 161, 103–125. https://doi.org/10.1016/S0009-2541(99)00083-2

Holdgate and Baker, 1979. The South Sandwich Islands: I. General description (Vol. 91). British Antarctic Survey, Scientific Reports, No. 91.

Kemp and Nelson, 1931. The South Sandwich Islands. 'Discovery' Reports, 3, 133-198.

Kern, C., Lübcke, P., Bobrowski, N., Campion, R., Mori, T., Smekens, J.-F., Stebel, K., Tamburello, G., Burton, M., Platt, U., Prata, F., 2015. Intercomparison of SO2 camera systems for imaging volcanic gas plumes. Journal of Volcanology and Geothermal Research 300, 22–36. https://doi.org/10.1016/j.jvolgeores.2014.08.026

Lachlan-Cope, T., Smellie, J.L., Ladkin, R., 2001. Discovery of a recurrent lava lake on Saunders Island (South Sandwich Islands) using AVHRR imagery. Journal of Volcanology and Geothermal Research 112, 105–116. https://doi.org/10.1016/S0377-0273(01)00237-2

Lamur, A., Lavallée, Y., Iddon, F.E., Hornby, A.J., Kendrick, J.E., von Aulock, F.W., Wadsworth, F.B., 2018. Disclosing the temperature of columnar jointing in lavas. Nature Communications 9, 1432. https://doi.org/10.1038/s41467-018-03842-4

Larter, R.D., Vanneste, L.E., Morris, P., Smythe, D.K., 2003. Structure and tectonic evolution of the South Sandwich arc. Geological Society, London, Special Publications 219, 255–284. https://doi.org/10.1144/GSL.SP.2003.219.01.13

Lawver, L.A., Dick, H.J.B., 1983. The American-Antarctic Ridge. Journal of Geophysical Research: Solid Earth 88, 8193–8202. https://doi.org/10.1029/JB088iB10p08193

Leat, P.T., Day, S.J., Tate, A.J., Martin, T.J., Owen, M.J., Tappin, D.R., 2013. Volcanic evolution of the South Sandwich volcanic arc, South Atlantic, from multibeam bathymetry. Journal of Volcanology and Geothermal Research 265, 60–77. https://doi.org/10.1016/j.jvolgeores.2013.08.013

Leat, P.T., Fretwell, P.T., Tate, A.J., Larter, R.D., Martin, T.J., Smellie, J.L., Jokat, W., Bohrmann, G., 2016. Bathymetry and geological setting of the South Sandwich Islands volcanic arc. Antarctic Science 28, 293–303. https://doi.org/10.1017/S0954102016000043

Leat, P.T., Pearce, J.A., Barker, P.F., Millar, I.L., Barry, T.L., Larter, R.D., 2004. Magma genesis and mantle flow at a subducting slab edge: the South Sandwich arc-basin system. Earth and Planetary Science Letters 227, 17–35. https://doi.org/10.1016/j.epsl.2004.08.016

Leat, P.T., Smellie, J.L., Millar, I.L., Larter, R.D., 2003. Magmatism in the South Sandwich arc. Geological Society, London, Special Publications 219, 285–313. https://doi.org/10.1144/GSL.SP.2003.219.01.14

Leat, P.T., Tate, A.J., Tappin, D.R., Day, S.J., Owen, M.J., 2010. Growth and mass wasting of volcanic centers in the northern South Sandwich arc, South Atlantic, revealed by new multibeam mapping. Marine Geology 275, 110–126. https://doi.org/10.1016/j.margeo.2010.05.001

LeMasurier, W.E., Thomson, J.W., Baker, P.E., Kyle, P.R., Rowley, P.D., Smellie, J.L., Verwoerd, W.J., 1990. Volcanoes of the Antarctic Plate and Southern Ocean, Volcanoes of the Antarctic Plate and Southern Oceans. American Geophysical Union, Washington, D.C.

Linse, K., Copley, J.T., Connelly, D.P., Larter, R., Pearce, D.A., Polunin, N.V.C., Rogers, A.D., Chen, C., Clarke, A., Glover, A.G., Graham, A.G.C., Huvenne, V.A.I., Marsh, L., Reid, W.D.K., Roterman, C.N., Sweeting, C.J., Zwirglmaier, K., Tyler, P.A., 2019. Fauna of the Kemp Caldera and its upper bathyal hydrothermal vents (South Sandwich Arc, Antarctica). Royal Society Open Science 6.

Liu, E.J., Cashman, K.V., Rust, A.C., Höskuldsson, A., 2017. Contrasting mechanisms of magma fragmentation during coeval magmatic and hydromagmatic activity: the Hverfjall Fires fissure eruption, Iceland. Bull Volcanol 79, 68. https://doi.org/10.1007/s00445-017-1150-8

Livermore, R., Cunningham, A., Vanneste, L., Larter, R., 1997. Subduction influence on magma supply at the East Scotia Ridge. Earth and Planetary Science Letters 150, 261–275. https://doi.org/10.1016/S0012-821X(97)00074-5

Lucas, B.D. and Kanade, T. 1981. An iterative image registration technique with an application to stereo vision. Proceedings DARPA Image Understanding Workshop, April 1981, 121-130.

Lynch, H.J., White, R., Naveen, R., Black, A., Meixler, M.S., Fagan, W.F., 2016. In stark contrast to widespread declines along the Scotia Arc, a survey of the South Sandwich Islands finds a robust seabird community. Polar Biol 39, 1615–1625. https://doi.org/10.1007/s00300-015-1886-6

Marine Protected Areas Order, 2013. S. R. & O. No: 1 of 2013.

Moore, J.G., 1967. Base surge in recent volcanic eruptions. Bull Volcanol 30, 337. https://doi.org/10.1007/BF02597678

876 Moretti, R., Papale, P., 2004. On the oxidation state and volatile behavior in multicomponent gas–
877 melt equilibria. Chemical Geology, 7th Silicate Melt Workshop 213, 265–280.
878 https://doi.org/10.1016/j.chemgeo.2004.08.048
879 Müller, C., 2001. Upper mantle seismic anisotropy beneath Antarctica and the Scotia Sea region.
880 Geophys J Int 147, 105–122. https://doi.org/10.1046/j.1365-246X.2001.00517.x
881 Müller, C., Bayer, B., Eckstaller, A., Miller, H., 2008. Mantle flow in the South Sandwich subduction
882 environment from source-side shear wave splitting. Geophysical Research Letters 35.
883 https://doi.org/10.1029/2007GL032411
884 Nemeth, K., Cronin, S.J., Charley, D.T., Harrison, M.J., Garae, E., 2006. Exploding lakes in Vanuatu
885 - "Surtseyan-style" eruptions witnessed on Ambae Island.
886 Ninkovich, D., Heezen, B.C., Conolly, J.R., Burckle, L.H., 1964. South Sandwich tephra in deep-sea
887 sediments. Deep Sea Research and Oceanographic Abstracts 11, 605–619.
888 https://doi.org/10.1016/0011-7471(64)90005-1
889 Patrick, M.R., Smellie, J.L., 2013. Synthesis A spaceborne inventory of volcanic activity in Antarctica
890 and southern oceans, 2000–10. Antarctic Science 25, 475–500.
891 https://doi.org/10.1017/S0954102013000436
892 Patrick, M.R., Smellie, J.L., Harris, A.J.L., Wright, R., Dean, K., Izbekov, P., Garbeil, H., Pilger, E.,
893 2005. First recorded eruption of Mount Belinda volcano (Montagu Island), South Sandwich
894 Islands. Bull Volcanol 67, 415–422. https://doi.org/10.1007/s00445-004-0382-6
895 Pearce, J.A., Baker, P.E., Harvey, P.K., Luff, I.W., 1995. Geochemical Evidence for Subduction
896 Fluxes, Mantle Melting and Fractional Crystallization Beneath the South Sandwich Island
897 Arc. J Petrology 36, 1073–1109. https://doi.org/10.1093/petrology/36.4.1073
898 Pearce, J.A., Barker, P.F., Edwards, S.J., Parkinson, I.J., Leat, P.T., 2000. Geochemistry and tectonic
899 significance of peridotites from the South Sandwich arc–basin system, South Atlantic.
900 Contrib Mineral Petrol 139, 36–53. https://doi.org/10.1007/s004100050572
901 Phillips, J.C., Humphreys, M.C.S., Daniels, K.A., Brown, R.J., Witham, F., 2013. The formation of
902 columnar joints produced by cooling in basalt at Staffa, Scotland. Bull Volcanol 75, 715.
903 https://doi.org/10.1007/s00445-013-0715-4
904 Plank, T., 2014. The Chemical Composition of Subducting Sediments, in: Keeling, R.F. (Ed.),
905 Treatise on Geochemistry. Elsevier, Amsterdam, pp. 607–629.
906 Plank, T., 2005. Constraints from Thorium/Lanthanum on Sediment Recycling at Subduction Zones
907 and the Evolution of the Continents. J Petrology 46, 921–944.
908 https://doi.org/10.1093/petrology/egi005
909 Plank, T., Langmuir, C.H., 1998. The chemical composition of subducting sediment and its
910 consequences for the crust and mantle. Chemical Geology 145, 325–394.
911 https://doi.org/10.1016/S0009-2541(97)00150-2
912 Plank, T., Manning, C.E., 2019. Subducting carbon. Nature 574, 343–352.
913 https://doi.org/10.1038/s41586-019-1643-z
914 Roberts, S.J., Monien, P., Foster, L.C., Loftfield, J., Hocking, E.P., Schnetger, B., Pearson, E.J.,
915 Juggins, S., Fretwell, P., Ireland, L., Ochyra, R., Haworth, A.R., Allen, C.S., Moreton, S.G.,
916 Davies, S.J., Brumsack, H.-J., Bentley, M.J., Hodgson, D.A., 2017. Past penguin colony
917 responses to explosive volcanism on the Antarctic Peninsula. Nature Communications 8,
918 14914. https://doi.org/10.1038/ncomms14914
919 Sano, Y., Marty, B., 1995. Origin of carbon in fumarolic gas from island arcs. Chemical Geology 119,
920 265–274. https://doi.org/10.1016/0009-2541(94)00097-R
921 Shinohara, H., 2013. Composition of volcanic gases emitted during repeating Vulcanian eruption
922 stage of Shinmoedake, Kirishima volcano, Japan. Earth, Planets and Space 65, 17.
923 Shinohara, H., 2005. A new technique to estimate volcanic gas composition: plume measurements
924 with a portable multi-sensor system. Journal of Volcanology and Geothermal Research 143,
925 319–333. https://doi.org/10.1016/j.jvolgeores.2004.12.004
926 Smalley, R., Dalziel, I.W.D., Bevis, M.G., Kendrick, E., Stamps, D.S., King, E.C., Taylor, F.W.,
927 Lauría, E., Zakrajsek, A., Parra, H., 2007. Scotia arc kinematics from GPS geodesy.
928 Geophysical Research Letters 34. https://doi.org/10.1029/2007GL031699
929 Smellie, J.L., 1999. The upper Cenozoic tephra record in the south polar region: a review. Global and
930 Planetary Change 21, 51–70. https://doi.org/10.1016/S0921-8181(99)00007-7

Smellie, J.L., Morris, P., Leat, P.T., Turner, D.B., Houghton, D., 1998. Submarine caldera and other volcanic observations in Southern Thule, South Sandwich Islands. Antartic science 10, 171–172. https://doi.org/10.1017/S0954102098000224

Sohn, Y.K., Chough, S.K., 1989. Depositional processes of the Suwolbong tuff ring, Cheju Island (Korea). Sedimentology 36, 837–855. https://doi.org/10.1111/j.1365-3091.1989.tb01749.x

Spry, A., 1962. The origin of columnar jointing, particularly in basalt flows. Journal of the Geological Society of Australia 8, 191–216. https://doi.org/10.1080/14400956208527873

Symonds, R.B., Gerlach, T.M., Reed, M.H., 2001. Magmatic gas scrubbing: implications for volcano monitoring. Journal of Volcanology and Geothermal Research 108, 303–341. https://doi.org/10.1016/S0377-0273(00)00292-4

Tamburello, G., 2015. Ratiocalc: Software for processing data from multicomponent volcanic gas analyzers. Computers & Geosciences 82, 63–67. https://doi.org/10.1016/j.cageo.2015.05.004

Thomas, C., Livermore, R., Pollitz, F., 2003. Motion of the Scotia Sea plates. Geophys J Int 155, 789–804. https://doi.org/10.1111/j.1365-246X.2003.02069.x

Tonarini, S., Leeman, W.P., Leat, P.T., 2011. Subduction erosion of forearc mantle wedge implicated in the genesis of the South Sandwich Island (SSI) arc: Evidence from boron isotope systematics. Earth and Planetary Science Letters 301, 275–284. https://doi.org/10.1016/j.epsl.2010.11.008

Vanneste, L.E., Larter, R.D., 2002. Sediment subduction, subduction erosion, and strain regime in the northern South Sandwich forearc: Northern South Sandwich Forearc. J. Geophys. Res. 107. https://doi.org/10.1029/2001JB000396

Vervoort, J.D., Plank, T., Prytulak, J., 2011. The Hf–Nd isotopic composition of marine sediments. Geochimica et Cosmochimica Acta 75, 5903–5926. https://doi.org/10.1016/j.gca.2011.07.046

Waters, A.C., Fisher, R.V., 1971. Base surges and their deposits: Capelinhos and Taal Volcanoes. Journal of Geophysical Research: Solid Earth 5596–5614. https://doi.org/10.1029/JB076i023p05596@10.1002/(ISSN)2169-9356.METIV1

Wohletz, K.H., Sheridan, M.F., 1983. Hydrovolcanic explosions; II, Evolution of basaltic tuff rings and tuff cones. Am J Sci 283, 385–413. https://doi.org/10.2475/ajs.283.5.385.

Supplementary Table S1

Supplementary Table S2

Click here to access/download

Supplementary Material

Supplementary_Table_2_GasData.xlsx

Click here to access/download

Supplementary Material

Supplementary_Table_3_CarbonIsotopeData.xlsx

Supplementary Table S4